# Joint Waveform and Receive Filter Design for Pulse Compression in Weather Radar Systems

Mohammad Alaee-Kerahroodi, *Senior Member, IEEE,* Linlong Wu, *Member, IEEE,* Ehsan Raei, *Member, IEEE,*
M. R. Bhavani Shankar, *Senior Member, IEEE*

*Abstract*—The meteorological industry is currently exploring Solid State Weather Radar (SSWR) systems, a new technology that emits minimal transmission power, to minimize harm to the environment and reduce system cost. However, accurately estimating reflectivity for each polarization and decreasing the blind range present significant challenges for SSWR systems that use pulse compression. In these systems, transmit waveforms and receive filters play a crucial role in enhancing estimation accuracy, while implementing partial correlation can reduce the blind range. In this research, we propose a novel joint design technique for transmit waveforms and receive filters in weather radar systems using the Alternating Direction Method of Multipliers (ADMM) and Coordinate Descent (CD) optimization approaches. We demonstrate the effectiveness of our technique by iteratively solving nonconvex design problems and showcasing the convergence of the objective function. Furthermore, we assess the impact of our proposed waveform and receive filter, as well as the blind range, on dual-polarized real weather radar data, illustrating the practicality of our approach. Our research provides a promising solution for the challenges faced by SSWR systems and offers a sustainable and efficient solution for the industry's needs.

*Keywords*—ADMM, CD, ISL, PSL, MSE, blind range, pulse compression, weather radar.

## I. Introduction

Pulse compression is a technique used in modern radar systems to achieve high range resolution while reducing the peak transmitting power. This technique involves transmitting a long modulated waveform and obtaining the same range resolution as an unmodulated short pulse, which enables the radar system to discriminate targets with high accuracy even in the presence of noise and clutter. The technique was first proposed in the 1950s, and it has since been developed and refined in many different forms [1]–[6]. However, its application in weather radar systems is yet limited.

### A. Reflectivity and Power

In radar systems, "power" refers to the strength of the signal that is transmitted. In general, higher power levels can result in stronger signals being returned from targets, which can improve the accuracy of target parameter estimation. In the receive side, the strength of the signal reflected from a target is often measured in terms of "reflectivity". Reflectivity is a function of the physical characteristics of the target, such as size, shape, and composition. The higher the reflectivity of a target, the stronger the signal that is returned to the radar system.

In meteorology, reflectivity is commonly used to estimate the intensity of precipitation. In particular, the reflectivity factor $Z$ is proportional to the sixth power of the precipitation particle diameter. However, the relationship between reflectivity and precipitation is not always straightforward due to factors such as attenuation, variations in the particle size distribution, and the presence of non-precipitation echoes. The ultimate goal of a weather radar is to improve the accuracy of precipitation estimation by mitigating these factors and reducing the effects of noise and clutter. Higher reflectivity values are generally associated with more intense precipitation, such as heavy rain or hail.

### B. Pulse Compression in Weather Radar Systems

Pulse compression technology used in solid state weather radar (SSWR) provides several benefits compared to conventional high-power short-pulse magnetron radars, as long as accurate reflectivity estimation is ensured. These advantages include lower peak power, improved phase stability (comparable to Klystron radars), reduced weight, and enhanced range resolution, as reported in various studies [7]–[9]. However, using pulse compression in weather radar systems, poses a number of challenges for weather radar systems, the majority of which come from increasing of the blind range and the autocorrelation sidelobe levels [9]–[11].

*a) Blind Range:* In order to achieve sensitivity comparable to a high-power short-pulse radar using a low-power SSWR, a long transmit waveform must be utilized. As a consequence of using long transmitting waveforms, the blind range, associated with blanking the receiver whilst transmitting the signal, will increase and shorter ranges will not be covered. A solution to decrease the blind range is the use of concatenated waveforms, which incorporates a combination of longer sub-pulses for long range and shorter sub-pulses for short range and provides simultaneous radar coverage for both short and long ranges [12], [13]. Although the concatenated waveforms have a number of attractive attributes, they present a challenging problem in that different sub-pulses will reflect back from different ranges and be received at the same time. Therefore since each sub-pulse is not separable at the RF front-end, a more complex radio-frequency (RF) chain is required [12],

[14]. An alternative to the concatenated waveforms solution is computing partial correlation between the transmitted signal and received reflections. This technique is called progressive pulse compression (PPC), and is based on partial decoding of the received signal after the transmission time. The technique has been tested with real weather radar data of PX-1000 in [15], and it offers several advantages over concatenated waveforms. In fact, the transmit waveform will be superposed with the echos even when the receiver is turned off (during the transmission). Depending on the waveform duration, a portion of the waveform that is reflected by the weather targets (if existent) will be received as soon as the receiver is turned on (after the transmission time). This portion can be used for partial correlation.

*b) Sidelobe Levels:* In addition to the blind range issue, targets in weather radar systems are extended volume scatterers, with range sidelobes being a significant source of error for meteorological parameter estimation [14]. To achieve waveforms with extremely low sidelobe levels, two design strategies are widely pursued; one aiming to maximize the signal to noise ratio (SNR) of the received signal, through the use of matched filter design [14], [16], while the other achieving low estimation error on meteorological scattering coefficient by minimizing the reflectivity parameter's mean-squared error (MSE) or, alternatively, increasing the received signal's signal to interference plus noise ratio (SINR) through the design of the receive mismatched filter [5], [17]–[24]. Indeed, the matched filter improves the SNR of the target when it is contaminated with white Gaussian noise, whereas mismatched filter improves the signal to sidelobe ratio by increasing the filter length.

### C. Background

Previous works, such as [17] and [25], have used gradient-based approaches to address the filter design problem for mismatch peak sidelobe level (PSL) and integrated sidelobe level (ISL) metrics. However, they only consider the minimization of the $\ell_p$-norm metric of autocorrelation sidelobes for even values of $p$. On the other hand, [24] proposes a majorization-minimization (MM)-based approach for joint waveform and filter design, where a surrogate function of the original objective function is minimized. Despite the fact that the problem of designing waveforms with low sidelobe levels has been addressed in a number of recent studies (see, for instance, [6], [8], [13], [14], [16], [17], [24]–[43]), they need to be revisited due to the challenging need for accurate amplitude and phase estimation of the reflected signal in a pulse compression weather radar system. In this context, designing the mismatched receive filter concurrently with optimizing the transmit waveform can result in an extremely small correlation sidelobes with a negligible SNR loss as reported in [9], [14], [16], [24], [38], [40], [42].

In contrast to aforementioned methods, this paper introduces a novel approach based on coordinate descent (CD) for solving the joint design problem, which guarantees monotonic convergence of the original objective function and allows for finding an optimum solution for any $p \geq 2$. Moreover, this approach

can be used for discrete-phase signal design, resulting in a waveform that can be directly implemented in a digital system, as shown in [44], [45]. Notably, [36] used CD framework for designing waveforms in multiple input multiple output (MIMO) radar systems. In contrast to this paper, in the current study we consider the problem of mismatched filter design together with the waveform design problem. The current study also considers minimizing the MSE metric to reduce the estimation error of the scattering coefficient, in addition to the PSL/ISL metrics, which is not reported in [36]. Unlike [46] that uses a gradient-based approach for MSE optimization, this study proposes an Alternating Direction Method of Multipliers (ADMM)-based solution with monotonic convergence properties. Furthermore, unlike [47] that focuses on slow-time waveform and filter design based on ADMM, this study designs fast-time waveform and filter pairs.

### D. Contribution

In the present study, we focus on the two aforementioned issues of blind range and autocorrelation sidelobe level reduction in pulse compression weather systems. Regarding the former, we show that the adoption of an integrated sidelobe level-based metric such as mismatched ISL can counteract the influence of blind range on the optimization procedure, which can lead to more refined outcomes following calibration of the partial correlation outputs in the blind range. For the latter issue, we formulate the optimization problems of joint waveform and filter design for weather radar systems, using mismatch PSL, mismatch ISL, and MSE objective functions. We show that the mismatched PSL/ISL metrics do not require noise variance estimation, while the MSE metric does. All of them, however, will obtain small sidelobe levels in the autocorrelation sidelobes. Following the description of the aforementioned problems, we propose various optimization techniques based on CD and ADMM to solve the problems and obtain a pair of optimized waveform and filter. Then, using the optimized waveform and filter pair, we evaluate the performance of the chosen metric and its corresponding optimization solution on actual weather radar data. The contributions of this study is summarized as follows:

- The problem of joint waveform and filter design for weather radar systems is formulated using mismatch PSL, mismatch ISL, and MSE metrics. It is shown that the mismatched PSL/ISL metrics do not require noise variance estimation, while the MSE metric does.
- An optimization framework based on CD is proposed for joint waveform and receive filter design using $\ell_p$-norm criteria. It has a monotonic convergence of the objective function.
- An ADMM-based optimization framework has been proposed for the MSE metric, resulting in monotonic improvement of the objective function.
- Partial correlation is used as an alternative to concatenating waveforms to reduce weather radar blind range. The results show that using an integrated sidelobe level-based metric such as mismatched ISL can counteract the influence of blind range on the optimization procedure,

leading to more refined outcomes following calibration of the partial correlation outputs in the blind range.

- Several numerical examples have been used to demonstrate the proposed technique's impact on real dual polarized weather radar $I$ and $Q$ data in terms of estimating the relevant weather parameters.

The current study assume that the coded pulse utilizes the same bandwidth as the uncoded pulse. Additionally, since the simulation is conducted in the digital domain, any range misalignment between the convolved and sampled signals is not taken into account. In other words, it is assumed that the sampling process is ideal, and that the signal bandwidth (and therefore range resolution) remains unchanged after pulse compression. However, as mentioned in [48], [49], weather radars that use pulse compression typically require range-oversampling processing in practice.

### E. Organization and Notations

The rest of this paper is organized as follows. In Section II, we formulate different optimization problems for waveform and receive filter design which enables the use of pulse compression in weather radar systems. We develop an algorithm based on the ADMM framework in Section III to identify the solution of joint waveform and filter design based on MSE metric. In IV, we look at a PSL and ISL based metric to find the solution to the optimization problem using CD framework. In Section V, we cover a variety of numerical experiments using both real radar data and simulated data to evaluate the efficiency of the proposed algorithms. Finally, Section VI concludes the paper.

*Notation:* Boldface upper case letters denote matrices, boldface lower case letters denote column vectors, and italics denote scalars. $\mathbb{Z}$, $\mathbb{R}$ and $\mathbb{C}$ denote the integer, real and complex field, respectively. $\mathbb{E}\{.\}$ represents the mathematical expectation, also known as the expected value or the mean. $\text{Re}(\cdot)$ and $\text{Im}(\cdot)$ denote the real and imaginary part respectively. $\arg(\cdot)$ denotes the phase of a complex number. The superscripts $(\cdot)^T$, $(\cdot)^*$, and $(\cdot)^H$ denote transpose, complex conjugate, and conjugate transpose, respectively. $X_{i,j}$ denotes the $(i, j)^{th}$ element of a matrix and $x_i$ denotes the $i^{th}$ element of vector $\mathbf{x}$. $\text{vec}(\mathbf{x})$ is a column vector obtained by stacking all the columns of $\mathbf{x}$. Further, $\|\mathbf{x}\|$ is the $l_2$ norm of the vector $\mathbf{x}$.

## II. System Model and Problem Formulation

The goal of this work is to bring advances in joint radar waveform and filter design to the field of weather sensing by using pulse compression to enable low-power and mobile solutions. To this end, in this section we present the system model and problem formulation required for signal design using matched and mismatched filters.

Let $\mathbf{J}_k$ be $N \times N$ shift matrix which its $(m, n)$-th entry $(m = 1, 2, \ldots, N, n = 1, 2, \ldots, N)$ is given by

$$\mathbf{J}_k(m, n) = \begin{cases} 1, & m - n = k \\ 0, & m - n \neq k. \end{cases} \tag{1}$$

Also, let $\mathbf{x} = [x_1, x_2, \ldots, x_N]^T \in \mathbb{C}^N$ be the transmitted fast-time radar code vector with $N$ being the number of coded

sub-pulses (code length). Then, the received signal $\mathbf{y} \in \mathbb{C}^N$ after sampling by Analog-to-digital converter (ADC) from the range bin of interest is [46], [50], [51],

$$\mathbf{y} = \alpha_0 \mathbf{x} + \underbrace{\sum_{\substack{k=-N+1 \\ k \neq 0}}^{N-1} \alpha_k \mathbf{J}_k \mathbf{x}}_{\text{interference caused by radar code}} + \nu, \tag{2}$$

where $\alpha_0$ is a complex-valued scalar, and $\alpha_k$ are proportional to the reflectivity of the adjacent range bins illuminated by the radar pulse compression code. In (2), $\nu \sim \mathcal{N}(\mathbf{0}, \sigma_\nu^2 \mathbf{I})$ is the noise vector which we assume that it is uncorrelated with the other signal-dependent terms. Further, we assume that the scatterer coefficients $\{\alpha_k\}_{k \neq 0}$ in (9) are independent of each other and of $\nu$, with

$$\mathbb{E}\{|\alpha_k|^2\} = \zeta, \quad k \neq 0. \tag{3}$$

The second term in (2) denotes interference caused by the radar code. Note that, in the conventional weather radars which do not employ pulse compression at the transmitter, the received signal will not contain this term.

In weather radar systems, an important step towards analyzing the hydrometer phenomena is the estimation of $\alpha_0$; this quantity is proportional to the reflectivity (of the scatterer) attenuated along the return path to the radar receiver at the range bin of interest. Suppose a linear finite impulse response receive filter $\mathbf{w} \in \mathbb{C}^N$ is deployed on the receive side. Then the output of the filter, corresponding to the maximum overlap, can be obtained by calculating $z = \mathbf{w}^H \mathbf{y}$. Depending on the selection of $\mathbf{w}$, matched and mismatched filtering approaches can be used to estimate $\alpha_0$.

### A. Matched Filtering

In this case, we set $\mathbf{w} = \mathbf{x}$, to obtain

$$z = \mathbf{x}^H \mathbf{y} = \alpha_0 \mathbf{x}^H \mathbf{x} + \sum_{\substack{k=-N+1 \\ k \neq 0}}^{N-1} \alpha_k \mathbf{x}^H \mathbf{J}_k \mathbf{x} + \mathbf{x}^H \nu. \tag{4}$$

Given $\|\mathbf{x}\|^2 = 1$, the estimate of $\alpha_0$ through matched filtering is given by [46], [50], [51],

$$\hat{\alpha}_0 = \mathbf{x}^H \mathbf{y}. \tag{5}$$

This estimation requires the absence of sidelobes, $\sum_{\substack{k=-N+1 \\ k \neq 0}}^{N-1} \alpha_k \mathbf{x}^H \mathbf{J}_k \mathbf{x}$, for the transmit waveform to ensure enhanced estimation of the reflectivity. Formally, the performance of the estimator in (4) is determined by the received SINR determined as follows

$$\text{SINR} = \frac{|\alpha_0|^2}{\zeta \sum_{\substack{k=-N+1 \\ k \neq 0}}^{N-1} |\mathbf{x}^H \mathbf{J}_k \mathbf{x}|^2 + \sigma_\nu^2}. \tag{6}$$

In (6), the term $\sum_{\substack{k=-N+1 \\ k \neq 0}}^{N-1} |\mathbf{x}^H \mathbf{J}_k \mathbf{x}|^2$ is the ISL of the waveform autocorrelation function which is a form of self-noise that reduces the effectiveness of the reflectively estimation.

Towards minimizing the sidelobes, the following optimization problem can be considered for the transmit waveform design,

$$\begin{cases} \underset{\mathbf{x}}{\text{minimize}} & \sum_{k=1}^{N-1} |\mathbf{x}^H \mathbf{J}_k \mathbf{x}|^2 \\ \text{subject to} & \mathbf{x} \in \Omega \end{cases} \tag{7}$$

where $\Omega$ is a set of constraints on the transmitting waveform, which is defined mathematically in the next section, and typically reflects the limits of high power amplifiers and digital synthesizers [52].

The problem in (7) is the classic ISL minimization for the radar systems, which has been well studied in several recent papers. See [6], [14], [25], [28], [30], [32]–[36], [53]–[60] and references therein. Even-though a significant reduction in ISL values for point targets can be achieved by using the methods proposed in the aforementioned literature, the remaining sidelobes for distributed targets may still not be acceptable for weather radar applications, as typically weather scatterers have a wide-spatial and temporal distribution. In fact, unlike other radar applications, weather sensing not only requires object detection but also precise parameter estimation in order to determine the weather type. As a result, a small sidelobe from the transmit waveform can be aggregated over a wide range of weather targets, resulting in a significant error in parameter estimation.

### B. Mismatched Filtering

The motivation behind the use of mismatched-filter-based method is to have relatively larger filter lengths compared to the transmitted sequence length so that the autocorrelation sidelobe energy can be spread over larger lag coefficients [14]. This approach offers additional flexibility since the sequences and filters can be separately optimized within a framework, to obtain higher reduction in the self-noise term of the received signal. Towards this, let us define

$$\widetilde{\mathbf{x}} = [\mathbf{0}_M^T, \mathbf{x}^T, \mathbf{0}_M^T]^T, \tag{8}$$

and let $\widetilde{\mathbf{w}} \in \mathbb{C}^{\widetilde{N}}$ be the receive filter, with $\widetilde{N} = 2M + N$, with $M \in \mathbb{Z}_+$. In this case, the received signal after filtering can be obtained by

$$\widetilde{z} = \alpha_0 \widetilde{\mathbf{w}}^H \widetilde{\mathbf{x}} + \sum_{\substack{k=-\widetilde{N}+1 \\ k \neq 0}}^{\widetilde{N}-1} \alpha_k \widetilde{\mathbf{w}}^H \widetilde{\mathbf{J}}_k \widetilde{\mathbf{x}} + \widetilde{\mathbf{w}}^H \widetilde{\nu}, \tag{9}$$

where $\widetilde{\mathbf{J}}_k$ is $\widetilde{N} \times \widetilde{N}$ shift matrix and can be defined similar to (1), i. e., its $(m,n)$-th entry is 1, when $m - n = k$, and 0 otherwise. Further, $\widetilde{\nu} \sim \mathcal{N}\left(\mathbf{0}, \sigma_{\widetilde{\nu}}^2 \mathbf{I}\right)$. The received SINR in this case is

$$\text{SINR} = \frac{|\alpha_0|^2 |\widetilde{\mathbf{w}}^H \widetilde{\mathbf{x}}|^2}{\widetilde{\mathbf{w}}^H \mathbf{R} \widetilde{\mathbf{w}}}, \tag{10}$$

where

$$\mathbf{R} = \zeta \sum_{\substack{k=-\widetilde{N}+1 \\ k \neq 0}}^{\widetilde{N}-1} \widetilde{\mathbf{J}}_k \widetilde{\mathbf{x}} \widetilde{\mathbf{x}}^H \widetilde{\mathbf{J}}_k^H + \sigma_{\widetilde{\nu}}^2 \mathbf{I}. \tag{11}$$

In this case, the instrumental variable estimate of $\alpha_0$ is given by [46], [50], [51],

$$\hat{\alpha}_0 = \frac{\widetilde{z}}{\widetilde{\mathbf{w}}^H \widetilde{\mathbf{x}}}, \tag{12}$$

and its MSE can be derived by [46],

$$\text{MSE}(\hat{\alpha}_0) = \mathbb{E}\left\{ \left| \frac{\widetilde{z}}{\widetilde{\mathbf{w}}^H \widetilde{\mathbf{x}}} - \alpha_0 \right|^2 \right\} = \frac{\widetilde{\mathbf{w}}^H \mathbf{R} \widetilde{\mathbf{w}}}{|\widetilde{\mathbf{w}}^H \widetilde{\mathbf{x}}|^2}. \tag{13}$$

Considering (10) and (13) we can readily observe that minimizing the MSE is equivalent with maximizing SINR.

The optimum filter which enhances the estimation of $\alpha_0$ can be obtained by solving the following optimization problem,

$$\underset{\widetilde{\mathbf{w}}}{\text{minimize}} \frac{\widetilde{\mathbf{w}}^H \mathbf{R} \widetilde{\mathbf{w}}}{|\widetilde{\mathbf{w}}^H \widetilde{\mathbf{x}}|^2}, \tag{14}$$

which yields to the following well-known closed-form expression minimum variance distortionless response (MVDR) solution for the optimized $\mathbf{w}$ vector,

$$\widetilde{\mathbf{w}}^\star = \mathbf{R}^{-1} \widetilde{\mathbf{x}}. \tag{15}$$

However, the above MSE-based filter design approach necessitates knowledge of $\sigma_{\widetilde{\nu}}^2$, which may be difficult to obtain for weather radar applications. Instead, the mismatch ISL and PSL discussed in the sequel do not require this knowledge. The use of a mismatched filter in radar signal processing typically does not alter the range resolution. Nevertheless, it can lead to a reduction in the SNR, which corresponds to the pulse compression gain of the received signal. This is because the mismatched filter is optimized for other signal processing aspects, such as sidelobe reduction, which may come at the expense of not achieving the maximum gain attainable by a matched filter. Hence, while range resolution remains largely unaffected, the performance of the radar system as a whole can be affected by the use of a mismatched filter.

### C. Mismatch ISL Minimization

A possible approach to enhance further the SINR is to optimize mismatch ISL, defined by [51]

$$\text{Mismatch ISL} = \sum_{\substack{k=-\widetilde{N}+1 \\ k \neq 0}}^{\widetilde{N}-1} \frac{|\widetilde{\mathbf{w}}^H \widetilde{\mathbf{J}}_k \widetilde{\mathbf{x}}|^2}{|\widetilde{\mathbf{w}}^H \widetilde{\mathbf{x}}|^2}. \tag{16}$$

By this minimization, we guarantee that $\hat{\alpha}_0$ in (12) is an enhanced estimate of $\alpha$. To see the reasoning, let us calculate

$$\hat{\alpha}_0 - \alpha_0 = \sum_{\substack{k=-\widetilde{N}+1 \\ k \neq 0}}^{\widetilde{N}-1} \alpha_k \frac{\widetilde{\mathbf{w}}^H \widetilde{\mathbf{J}}_k \widetilde{\mathbf{x}}}{\widetilde{\mathbf{w}}^H \widetilde{\mathbf{x}}} + \frac{\widetilde{\mathbf{w}}^H \widetilde{\nu}}{\widetilde{\mathbf{w}}^H \widetilde{\mathbf{x}}}. \tag{17}$$

By defining Inverse Signal to Noise Ratio (ISNR),

$$\text{ISNR} = \frac{\|\widetilde{\mathbf{w}}\|^2}{|\widetilde{\mathbf{w}}^H \widetilde{\mathbf{x}}|^2}, \tag{18}$$

under white-noise assumption, the variance of the noise-dependent term in (17) equals $\sigma_{\widetilde{\nu}}^2$ ISNR. This means that

when $\sigma_\nu^2$ and $\alpha_k$ are unknown, the minimization of the data-independent term of the above estimator is a natural way of minimizing the MSE. This can be obtained by

$$
\begin{cases}
\underset{\widetilde{\mathbf{x}},\widetilde{\mathbf{w}}}{\text{minimize}} & \dfrac{\sum_{\substack{k=-\widetilde{N}+1 \\ k\neq 0}}^{\widetilde{N}-1} |\widetilde{\mathbf{w}}^H \widetilde{\mathbf{J}}_k \widetilde{\mathbf{x}}|^2}{|\widetilde{\mathbf{w}}^H \widetilde{\mathbf{x}}|^2} \\
\text{subject to} & \mathbf{x} \in \Omega
\end{cases}
\tag{19}
$$

This problem is essentially a joint design of transmit waveform and receive filter weights, a problem which is studied in the literature [46], [61]–[72]. Meanwhile, the MSE minimization can also be interpreted as a joint design problem as

$$
\begin{cases}
\underset{\widetilde{\mathbf{x}},\widetilde{\mathbf{w}}}{\text{minimize}} & \dfrac{\widetilde{\mathbf{w}}^H \mathbf{R} \widetilde{\mathbf{w}}}{|\widetilde{\mathbf{w}}^H \widetilde{\mathbf{x}}|^2} \\
\text{subject to} & \mathbf{x} \in \Omega
\end{cases}
\tag{20}
$$

with $\mathbf{R}$ defined in (11). In the context of hydrometric estimation in weather radar, the noise is weak compared to the reflectivity of hydrometric scatters, i.e. $\zeta \gg \sigma_\nu^2$. Therefore, minimizing the MSE can be reasonably achieved by solving the problem 19. Besides, as earlier mentioned, the MSE minimization requires prior information on the ambient noise, which is hard to obtain in practice for weather applications and thereby leads to a model mismatches. On the contrary, the ISL approach avoids such an issue and could yield more robust results especially when the noise information is barely known.

### D. Mismatch PSL Minimization

Another possible approach is to optimize the transmit waveform and its corresponding filter weights based on mismatch PSL minimization that minimizes the maximum error in the estimation of the reflectively parameter. The mismatch PSL can be defined by [20], [51],

$$
\text{Mismatch PSL} = \max_{\substack{k=-\widetilde{N}+1 \\ k\neq 0}}^{\widetilde{N}-1} \frac{|\widetilde{\mathbf{w}}^H \widetilde{\mathbf{J}}_k \widetilde{\mathbf{x}}|^2}{|\widetilde{\mathbf{w}}^H \widetilde{\mathbf{x}}|^2}.
\tag{21}
$$

In this case, the optimization problem can be written as,

$$
\begin{cases}
\underset{\widetilde{\mathbf{x}},\widetilde{\mathbf{w}}}{\text{minimize}} & \underset{k\neq 0}{\max} \dfrac{|\widetilde{\mathbf{w}}^H \widetilde{\mathbf{J}}_k \widetilde{\mathbf{x}}|^2}{|\widetilde{\mathbf{w}}^H \widetilde{\mathbf{x}}|^2} \\
\text{subject to} & \mathbf{x} \in \Omega
\end{cases}
\tag{22}
$$

which is a non-convex min-max optimization problem. The optimal solution for the problem in (22) can be obtained using block coordinate descent (BCD) and bi-section approaches [28], or Second-Order Cone Programming (SOCP) [51].

### E. Joint Waveform and Mismatch Filter Design based on $\ell_p$-Norm Metric

Since the objective in (22) is nonsmooth and potentially the problem is non-deterministic polynomial-time hard (NP-hard), replacing it with a differentiable and smooth function may provide higher quality and faster convergence results. Indeed, it has been shown that the $\ell_p$-norm of autocorrelation

sidelobes of the transmitting waveform is a very successful figure of merit that allows to trade-off between good PSL and ISL via different $p \geq 2$ values [28], [57]. Motivated by this observation, we define a new metric based on $\ell_p$-norm optimization of transmit waveform and receive filter which is

$$
\begin{cases}
\underset{\widetilde{\mathbf{x}},\widetilde{\mathbf{w}}}{\text{minimize}} & \displaystyle\sum_{\substack{k=-\widetilde{N}+1 \\ k\neq 0}}^{\widetilde{N}-1} \dfrac{|\widetilde{\mathbf{w}}^H \widetilde{\mathbf{J}}_k \widetilde{\mathbf{x}}|^p}{|\widetilde{\mathbf{w}}^H \widetilde{\mathbf{x}}|^2} \\
\text{subject to} & \mathbf{x} \in \Omega
\end{cases}
\tag{23}
$$

By considering the above optimization problem, different objective functions can be generated by changing the value of $p$ in (23). Precisely, $p = 2$ equals (19), and $p \to +\infty$ yields the problem in (22). Thus, this problem can be considered as a generalization form for mismatch ISL and PSL optimization problems. Section IV of this paper discusses the solution to (23), but before delving deeper into its details, let's fist consider the joint waveform and filter design problem based on the MSE metric in the following section.

It's worth noting that the waveform and filter design can be done offline, and pre-optimized pairs can be used in a practical radar system. Implementing this pair is as straightforward as implementing a matched filter, except that mismatched filter coefficients are used in the receive side instead of matched filter coefficients. Therefore, a fast-convolutional type algorithm can still be employed, where the optimized sequence obtained from one of the proposed algorithms in this paper is used as the transmit waveform, and the derived mismatch filter from this paper is used as the receive filter.

### III. ADMM-BASED WAVEFORM AND FILTER DESIGN FOR MSE MINIMIZATION

A possible solution for the problem in (20) is to alternatively optimize the transmit waveform and the receive filter by keeping the other variable fixed [19]. In this case, the design problem needs to have information about $\mathbf{R}$, which is considered to be obtained from a cognitive paradigm [73]. Some examples are the design algorithms referred to as the CREW (cognitive receiver and waveform) methods [46], which optimize the transmit sequence based on gradient solver and compute the optimum filter based on the MVDR solution. In this section, we propose a new solution to the optimization problem (20). The optimization problem in this case is:

$$
\begin{cases}
\underset{\widetilde{\mathbf{x}},\widetilde{\mathbf{w}}}{\text{minimize}} & \dfrac{\widetilde{\mathbf{w}}^H \left( \sum_{k=1}^K \mathbf{J}_k \widetilde{\mathbf{x}} \widetilde{\mathbf{x}}^H \mathbf{J}_k^H + \sigma^2 \mathbf{I} \right) \widetilde{\mathbf{w}}}{|\widetilde{\mathbf{w}}^H \widetilde{\mathbf{x}}|^2} \\
\text{subject to} & \mathbf{x} \in \Omega_\infty
\end{cases}
\tag{24}
$$

where $\Omega_\infty = \{\mathbf{x} \in \mathbb{C}^N | \ |x_i| = 1, \ i = 1,\ldots,N\}$. Using the alternative optimization approach [19], for a fixed $\widetilde{\mathbf{x}}$, the problem w.r.t $\widetilde{\mathbf{w}}$ is

$$
\underset{\widetilde{\mathbf{w}}}{\text{minimize}} \quad \frac{\widetilde{\mathbf{w}}^H \mathbf{R} \widetilde{\mathbf{w}}}{\widetilde{\mathbf{w}}^H \widetilde{\mathbf{x}} \widetilde{\mathbf{x}}^H \widetilde{\mathbf{w}}}
\tag{25}
$$

with $\mathbf{R} = \sum_{k=1}^{K} \mathbf{J}_k \widetilde{\mathbf{x}} \widetilde{\mathbf{x}}^H \mathbf{J}_k^H + \sigma^2 \mathbf{I}$, which is the classical MVDR problem and can be recast into

$$\begin{cases} \underset{\widetilde{\mathbf{w}}}{\text{minimize}} & \widetilde{\mathbf{w}}^H \mathbf{R} \widetilde{\mathbf{w}} \\ \text{subject to} & \widetilde{\mathbf{w}}^H \widetilde{\mathbf{x}} = 1 \end{cases} \tag{26}$$

Thus, the closed form solution of $\widetilde{\mathbf{w}}$ is given by

$$\widetilde{\mathbf{w}}^\star = \mathbf{R}^{-1} \widetilde{\mathbf{x}}, \tag{27}$$

and any scaled $\widetilde{\mathbf{w}}^\star$ is also optimal. For a fixed $\widetilde{\mathbf{w}}$, the problem w.r.t $\widetilde{\mathbf{x}}$ can be written as

$$\begin{cases} \underset{\widetilde{\mathbf{x}}}{\text{minimize}} & \dfrac{\widetilde{\mathbf{x}}^H \hat{\mathbf{P}} \widetilde{\mathbf{x}}}{\widetilde{\mathbf{x}}^H \hat{\mathbf{Q}} \widetilde{\mathbf{x}}} \\ \text{subject to} & |x_i| = 1, \end{cases} \tag{28}$$

where $\hat{\mathbf{P}} = \sum_{k=1}^{K} \mathbf{J}_k^H \widetilde{\mathbf{w}} \widetilde{\mathbf{w}}^H \mathbf{J}_k + \frac{\sigma^2}{N} \|\widetilde{\mathbf{w}}\|^2$ and $\hat{\mathbf{Q}} = \widetilde{\mathbf{w}} \widetilde{\mathbf{w}}^H$.

Recall that $\widetilde{\mathbf{x}} = [\mathbf{0}_M^T, \mathbf{x}^T, \mathbf{0}_M^T]^T$, the problem in (28) is essentially to optimize $\mathbf{x}$. Therefore, it can be written as

$$\begin{cases} \underset{\mathbf{x}}{\text{minimize}} & \dfrac{\mathbf{x}^H \mathbf{P} \mathbf{x}}{\mathbf{x}^H \mathbf{Q} \mathbf{x}} \\ \text{subject to} & |x_i| = 1, \end{cases} \tag{29}$$

with $\mathbf{P} = [\hat{\mathbf{P}}]_{M+1:M+N, M+1:M+N}$ and $\mathbf{Q} = [\hat{\mathbf{Q}}]_{M+1:M+N, M+1:M+N}$. Further, this problem can be written equivalently by introducing slack variables as

$$\begin{aligned} \underset{\mathbf{x}, \mathbf{y}, \mathbf{z}}{\text{minimize}} & \quad \frac{\mathbf{y}^H \mathbf{P} \mathbf{y}}{\mathbf{z}^H \mathbf{Q} \mathbf{z}} \\ \text{subject to} & \quad |x_i| = 1 \\ & \quad \widetilde{\mathbf{x}} = \mathbf{y} \\ & \quad \widetilde{\mathbf{x}} = \mathbf{z}. \end{aligned}$$

Its Lagrangian function is

$$\mathcal{L}(\mathbf{x}, \mathbf{y}, \mathbf{z}, \mathbf{u}, \mathbf{v}) = \frac{\mathbf{y}^H \mathbf{P} \mathbf{y}}{\mathbf{z}^H \mathbf{Q} \mathbf{z}} + \frac{\rho_1}{2} \|\mathbf{y} - \mathbf{x} + \mathbf{u}\|^2 + \frac{\rho_2}{2} \|\mathbf{z} - \mathbf{x} + \mathbf{v}\|^2. \tag{30}$$

By deploying the ADMM framework, at the $\ell$-th iteration, the ADMM update rules are as follows:

$$\begin{cases} \mathbf{x}_{\ell+1} = \arg \underset{|x_i|=1}{\min} \mathcal{L}(\mathbf{x}, \mathbf{y}_\ell, \mathbf{z}_\ell, \mathbf{u}_\ell, \mathbf{v}_\ell) & (a) \\ \mathbf{y}_{\ell+1} = \arg \underset{\mathbf{y}}{\min} \mathcal{L}(\mathbf{x}_{\ell+1}, \mathbf{y}, \mathbf{z}_\ell, \mathbf{u}_\ell, \mathbf{v}_\ell) & (b) \\ \mathbf{z}_{\ell+1} = \arg \underset{\mathbf{z}}{\min} \mathcal{L}(\mathbf{x}_{\ell+1}, \mathbf{y}_{\ell+1}, \mathbf{z}, \mathbf{u}_\ell, \mathbf{v}_\ell) & (c) \\ \mathbf{u}_{\ell+1} = \mathbf{u}_\ell + \mathbf{y}_{\ell+1} - \mathbf{x}_{\ell+1} & (d) \\ \mathbf{v}_{\ell+1} = \mathbf{v}_\ell + \mathbf{z}_{\ell+1} - \mathbf{x}_{\ell+1}. & (e) \end{cases} \tag{31}$$

In the following, we will focus on solving (31)-(a)(b)(c). For notation simplicity, we ignore the subscript $\ell$ and $\ell+1$, which can be inferred according to the context.

The problem in 31(a) reduces to

$$\begin{aligned} \underset{\mathbf{x}}{\text{minimize}} & \quad \mathbf{x}^H \mathbf{x} - \text{Re}(\mathbf{a}^H \mathbf{x}) \\ \text{subject to} & \quad |x_i| = 1, \end{aligned} \tag{32}$$

where $\mathbf{a} = \frac{2}{\rho_1 + \rho_2} [\rho_1 (\mathbf{y} + \mathbf{u}) + \rho_2 (\mathbf{z} + \mathbf{v})]$. Since $\mathbf{x}^H \mathbf{x} = N$, the optimal solution to problem (32) is

$$\mathbf{x} = e^{j \arg(\mathbf{a})}. \tag{33}$$

Similarly, problem (31)(b) can be further written as

$$\underset{\mathbf{y}}{\text{minimize}} \quad \mathbf{y}^H \tilde{\mathbf{P}} \mathbf{y} + \text{Re}(\mathbf{b}^H \mathbf{y})$$

with $\tilde{\mathbf{P}} = \frac{\mathbf{P}}{\mathbf{z}^H \mathbf{Q} \mathbf{z}} + \frac{\rho_1}{2} \mathbf{I} \succ \mathbf{0}$ and $\mathbf{b} = \rho_1 (\mathbf{u} - \mathbf{x})$. The closed form solution is

$$\mathbf{y} = -\frac{1}{2} \tilde{\mathbf{P}}^{-1} \mathbf{b}. \tag{34}$$

Finally, the problem (31)(c) can be recast as

$$\underset{\mathbf{z}}{\text{minimize}} \quad \left( \mathbf{z}^H \tilde{\mathbf{Q}} \mathbf{z} \right)^{-1} + \frac{\rho_2}{2} \mathbf{z}^H \mathbf{z} + \text{Re}(\mathbf{c}^H \mathbf{z}) \tag{35}$$

with $\tilde{\mathbf{Q}} = \frac{\mathbf{Q}}{\mathbf{y}^H \mathbf{P} \mathbf{y}} \succeq \mathbf{0}$ with rank 1 and $\mathbf{c} = \rho_2 (\mathbf{v} - \mathbf{x})$. By letting $\tilde{\mathbf{Q}} = \mathbf{U}^H \mathbf{\Lambda} \mathbf{U}$ with $\mathbf{U} \mathbf{U}^H = \mathbf{U}^H \mathbf{U} = \mathbf{I}$, $\tilde{\mathbf{c}} = \mathbf{U} \mathbf{c}$, and $\tilde{\mathbf{z}} = \mathbf{U} \mathbf{z}$, problem (35) can be equivalently expressed as

$$\underset{\tilde{\mathbf{z}}}{\text{minimize}} \quad \left( \tilde{\mathbf{z}}^H \mathbf{\Lambda} \tilde{\mathbf{z}} \right)^{-1} + \frac{\rho_2}{2} \tilde{\mathbf{z}}^H \tilde{\mathbf{z}} + \text{Re}(\tilde{\mathbf{c}}^H \tilde{\mathbf{z}}). \tag{36}$$

Since rank$\left( \tilde{\mathbf{Q}} \right) = 1$, we know that $\mathbf{\Lambda} = \text{diag}\left( \{\lambda_i\}_{i=1}^N \right)$ with $\lambda_1 = \frac{\|\widetilde{\mathbf{w}}\|^2}{\mathbf{y}^H \mathbf{P} \mathbf{y}}$ and $\lambda_2 = \cdots = \lambda_N = 0$. Thus, the objective function of problem (35), denoted by $f(\tilde{\mathbf{z}})$, can be expressed as

$$\begin{aligned} f(\tilde{\mathbf{z}}) = & \left\{ \left( \lambda_1 |\tilde{z}_1|^2 \right)^{-1} + \frac{\rho_2}{2} |\tilde{z}_1|^2 + \text{Re}(\tilde{c}_1^* \tilde{z}_1) \right\} \\ & + \left\{ \frac{\rho_2}{2} \hat{\mathbf{z}}^H \hat{\mathbf{z}} + \text{Re}(\hat{\mathbf{c}}^H \hat{\mathbf{z}}) \right\}, \end{aligned} \tag{37}$$

where $\tilde{z}_i$ is the $i$-th element of $\tilde{\mathbf{z}}$, $\hat{\mathbf{z}} = [\tilde{z}_2, \ldots, \tilde{z}_N]^T$ and $\hat{\mathbf{c}} = [\tilde{c}_2, \ldots, \tilde{c}_N]^T$.

Therefore, problem (36) can be decomposed into two independent problems. The first problem is as follows:

$$\underset{\tilde{z}_1}{\text{minimize}} \quad \left( \lambda_1 |\tilde{z}_1|^2 \right)^{-1} + \frac{\rho_2}{2} |\tilde{z}_1|^2 + \text{Re}(\tilde{c}_1^* \tilde{z}_1). \tag{38}$$

Since $\text{Re}(\tilde{c}_1^* \tilde{z}_1) \geq -|\tilde{c}_1| |\tilde{z}_1|$ with the equality achieved when $\arg(\tilde{z}_1) = \pi + \arg(\tilde{c}_1)$. Then, solving problem (38) is essentially solving

$$\underset{\tilde{z}_1}{\text{minimize}} \quad \left( \lambda_1 |\tilde{z}_1|^2 \right)^{-1} + \frac{\rho_2}{2} |\tilde{z}_1|^2 - |\tilde{c}_1| |\tilde{z}_1|. \tag{39}$$

Let $t = |\tilde{z}_1| \geq 0$ and $g(t) = \frac{1}{\lambda_1 t^2} + \frac{\rho_2}{2} t^2 - |\tilde{c}_1| t$, then the first-order optimality condition is

$$\rho_2 t^4 - |\tilde{c}_1| t^3 - \frac{2}{\lambda_1} = 0. \tag{40}$$

According to Descartes' rule of signs, we obtain the only positive root of the quartic polynomial equation. Hence, the optimal solution is $\tilde{z}_1 = -t e^{j \arg(\tilde{c}_1)}$.

The second problem is as follows:

$$\underset{\hat{\mathbf{z}}}{\text{minimize}} \quad \frac{\rho_2}{2} \hat{\mathbf{z}}^H \hat{\mathbf{z}} + \text{Re}(\hat{\mathbf{c}}^H \hat{\mathbf{z}}), \tag{41}$$

which has a closed form solution $\hat{\mathbf{z}} = -\frac{1}{\rho_2}\hat{\mathbf{c}}$. Finally, the optimal solution of problem (36) is

$$\tilde{\mathbf{z}} = \left[ -te^{j\arg(\tilde{c}_1)}, -\frac{\tilde{c}_2}{\rho_2}, \ldots, -\frac{\tilde{c}_N}{\rho_2} \right]^T, \quad (42)$$

and the optimal solution to problem (35) is thereby is $\mathbf{z} = \mathbf{U}^H\tilde{\mathbf{z}}$. The proposed algorithm is summarized in Algorithm 1.

---

**Algorithm 1** ADMM - Monotonic MSE Improvement for Joint Waveform and Filter Design

---

**Input:** $\rho_1, \rho_2$
**Output:** $\mathbf{x}, \widetilde{\mathbf{w}}$
1: set $n \leftarrow 0$
2: **repeat**
3:      $\mathbf{R} = \sum_{k=1}^{K} \mathbf{J}_k\widetilde{\mathbf{x}}\widetilde{\mathbf{x}}^H\mathbf{J}_k^H + \sigma^2\mathbf{I}$
4:      $\widetilde{\mathbf{w}}_{n+1} = \mathbf{R}^{-1}\widetilde{\mathbf{x}}_n,$
5:      $\hat{\mathbf{P}} = \sum_{k=1}^{K} \mathbf{J}_k^H\widetilde{\mathbf{w}}_{n+1}\widetilde{\mathbf{w}}_{n+1}^H\mathbf{J}_k + \frac{\sigma^2}{N}\|\widetilde{\mathbf{w}}_{n+1}\|^2$
6:      $\hat{\mathbf{Q}} = \widetilde{\mathbf{w}}_{n+1}\widetilde{\mathbf{w}}_{n+1}^H$
7:      $\mathbf{P} = [\hat{\mathbf{P}}]_{M+1:M+N,M+1:M+N}$   and   $\mathbf{Q} = [\hat{\mathbf{Q}}]_{M+1:M+N,M+1:M+N}$
8:      set $\ell \leftarrow 0$
9:      **repeat**
10:          $\mathbf{a}_\ell = \frac{2}{\rho_1+\rho_2}[\rho_1(\mathbf{y}_\ell + \mathbf{u}_\ell) + \rho_2(\mathbf{z}_\ell + \mathbf{v}_\ell)]$
11:          $\mathbf{x}_{\ell+1} = e^{j\arg(\mathbf{a}_\ell)}$
12:          $\tilde{\mathbf{P}} = \frac{\mathbf{P}}{\mathbf{z}_\ell^H\mathbf{Q}\mathbf{z}_\ell} + \frac{\rho_1}{2}\mathbf{I}$
13:          $\mathbf{b}_\ell = \rho_1(\mathbf{u}_\ell - \mathbf{x}_{\ell+1})$
14:          $\mathbf{y}_{\ell+1} = -\frac{1}{2}\tilde{\mathbf{P}}^{-1}\mathbf{b}_\ell$
15:          $\tilde{\mathbf{Q}} = \frac{\mathbf{Q}}{\mathbf{y}_{\ell+1}^H\mathbf{P}\mathbf{y}_{\ell+1}} = \mathbf{U}^H\mathbf{\Lambda}\mathbf{U}$
16:          $\tilde{\mathbf{c}} = \rho_2\mathbf{U}(\mathbf{v}_\ell - \mathbf{x}_{\ell+1})$
17:          Solve $\rho_2 t^4 - |\tilde{c}_1|t^3 - \frac{2}{\lambda_1} = 0$ and find optimal $t$
18:          $\tilde{\mathbf{z}} = \left[ -te^{j\arg(\tilde{c}_1)}, -\frac{\tilde{c}_2}{\rho_2}, \ldots, -\frac{\tilde{c}_N}{\rho_2} \right]^T$
19:          $\mathbf{z}_{\ell+1} = \mathbf{U}^H\tilde{\mathbf{z}}$
20:          $\mathbf{u}_{\ell+1} = \mathbf{u}_\ell + \mathbf{y}_{\ell+1} - \mathbf{x}_{\ell+1}$
21:          $\mathbf{v}_{\ell+1} = \mathbf{v}_\ell + \mathbf{z}_{\ell+1} - \mathbf{x}_{\ell+1}$
22:          $\ell \leftarrow \ell + 1$
23:      **until** convergence
24:      $n \leftarrow n + 1$
25: **until** convergence

---

## IV. CD-Based Waveform Design and Mismatch ISL/PSL Minimization

In this part, we consider the following optimization problem

$$\mathcal{P}_{\widetilde{\mathbf{x}},\widetilde{\mathbf{w}}} \begin{cases} \underset{\widetilde{\mathbf{x}},\widetilde{\mathbf{w}}}{\text{minimize}} & \displaystyle\sum_{\substack{k=-\tilde{N}+1 \\ k\neq 0}}^{\tilde{N}-1} \frac{|\widetilde{\mathbf{w}}^H\widetilde{\mathbf{J}}_k\widetilde{\mathbf{x}}|^p}{|\widetilde{\mathbf{w}}^H\widetilde{\mathbf{x}}|^2} \\ \text{subject to} & \mathbf{x} \in \Omega_h \end{cases} \quad (43)$$

where $p \geq 2$, $h \in \{L, \infty\}$, and the constraints $\mathbf{x} \in \Omega_\infty$ and $\mathbf{x} \in \Omega_L$ identify continuous alphabet and finite alphabet codes, i. e., $\Omega_\infty = \{\mathbf{x} \in \mathbb{C}^N \mid |x_n| = 1, \ n = 1, \ldots, N\}$, and $\Omega_L = \{\mathbf{x} \in \mathbb{C}^N \mid x_n \in \{1, e^{j\frac{2\pi}{L}}, \ldots, e^{j\frac{2\pi(L-1)}{L}}\}, \ n = 1, \ldots, N\}$,

respectively. Note that in the optimization problem $\mathcal{P}_{\widetilde{\mathbf{x}},\widetilde{\mathbf{w}}}$, by choosing $p = 2$, the resulting optimized filter and sequence will have a small ISL, and by minimizing the $\ell_p$-norm when $p \to +\infty$, the optimized filter and sequence will have a small PSL. To obtain the optimum solution of (43), we observe that the constraints are separable with respect to the optimization variables $\widetilde{\mathbf{x}}$, and $\widetilde{\mathbf{w}}$. In this case, one possible solution is to use the classical *alternating optimization* method [19], where we iteratively optimize for $\widetilde{\mathbf{w}}$ maintaining $\widetilde{\mathbf{x}}$ fixed and vice-versa.

### A. Optimization of filter

By keeping $\widetilde{\mathbf{x}}$ fixed, the optimization problem is

$$\mathcal{P}_{\widetilde{\mathbf{w}}} \begin{cases} \underset{\widetilde{\mathbf{w}}}{\min} & \displaystyle\sum_{\substack{k=-\tilde{N}+1 \\ k\neq 0}}^{\tilde{N}-1} \frac{|\widetilde{\mathbf{w}}^H\widetilde{\mathbf{J}}_k\widetilde{\mathbf{x}}|^p}{|\widetilde{\mathbf{w}}^H\widetilde{\mathbf{x}}|^2} \end{cases} \quad (44)$$

By using MM framework, we can majorize $|\widetilde{\mathbf{w}}^H\widetilde{\mathbf{J}}_k\widetilde{\mathbf{x}}|^p$ by a quadratic function locally [57].

*Lemma 4.1:* Let $f(x) = x^p$ with $p \geq 2$ and $x \in [0, t]$. Then for any given $x_0 \in [0, t)$, $f(x)$ is majorized at $x_0$ over the interval $[0, t]$ by

$$u(x) = ax^2 + \left(px_0^{p-1} - 2ax_0\right)x + ax_0^2 - (p-1)x_0^p \quad (45)$$

with

$$a = \frac{t^p - x_0^p - px_0^{p-1}(t - x_0)}{(t - x_0)^2}. \quad (46)$$

*Proof:* See [57]. ∎

Let us define the operator $(\circledast)$ to denote the correlation. The mismatched filter output at lag $k$ is defined as

$$(\widetilde{\mathbf{w}} \circledast \widetilde{\mathbf{x}})_k \equiv \widetilde{r}_k = \widetilde{\mathbf{w}}^H\widetilde{\mathbf{J}}_k\widetilde{\mathbf{x}}, \quad (47)$$

$k \in \{-M - N + 1, \ldots, N + M - 1\}$. Given $|\widetilde{r}_k^{(\ell)}|$ at the $\ell$-th iteration, according to Lemma 4.1, $|\widetilde{r}_k|^p$ is majorized at $|\widetilde{r}_k^{(\ell)}|$ over $[0, t]$ by

$$u(|\widetilde{r}_k|) = \tau_k|\widetilde{r}_k|^2 + \lambda_k|\widetilde{r}_k| + \gamma_k, \quad (48)$$

where[1]

$$\tau_k = \frac{t^p - |\widetilde{r}_k^{(\ell)}|^p - p|\widetilde{r}_k^{(\ell)}|^{p-1}\left(t - |\widetilde{r}_k^{(\ell)}|\right)}{\left(t - |\widetilde{r}_k^{(\ell)}|\right)^2}, \quad (49)$$

$$\lambda_k = p|\widetilde{r}_k^{(\ell)}|^{p-1} - 2\tau_k|\widetilde{r}_k^{(\ell)}|, \quad (50)$$

$$\gamma_k = \left(\tau_k|\widetilde{r}_k^{(\ell)}|^2 - (p-1)|\widetilde{r}_k^{(\ell)}|^p\right). \quad (51)$$

As illustrated above, (48) is the local majorizer over $[0, t]$, and we need to find a value of $t$ so that the objective is guaranteed to decrease. Now, let us observe that, $|\widetilde{r}_k| \leq \left(\sum_{k\neq 0} |\widetilde{r}_k^{(\ell)}|^p\right)^{\frac{1}{p}}$. Therefore, we can choose $t = \left(\sum_{k\neq 0} |\widetilde{r}_k^{(\ell)}|^p\right)^{\frac{1}{p}}$ in (49), and

---

[1]$a_k$ and $b_k$ depend on $\ell$, but the dependency is not depicted for the notational simplicity.

denoting by $\tau_k$, $\lambda_k$ and $\gamma_k$ the resulting coefficients, a surrogate function to $|\widetilde{r}_k|^p$ can be written as,

$$\sum_{k\neq 0} \left( \tau_k |\widetilde{r}_k|^2 + \lambda_k |\widetilde{r}_k| + \gamma_k \right). \tag{52}$$

Thus, the optimization problem is

$$\underset{\widetilde{\mathbf{w}}}{\text{minimize}} \sum_{k\neq 0} \frac{\tau_k |\widetilde{r}_k|^2 + \lambda_k |\widetilde{r}_k| \, \gamma_k}{|\widetilde{\mathbf{w}}^H \widetilde{\mathbf{x}}|^2} \tag{53}$$

Before proceeding further, notice that the second term in (52) can be majorized by [57],

$$\sum_{k\neq 0} \lambda_k |\widetilde{r}_k| \leq \sum_{k\neq 0} \lambda_k \text{Re}\left\{ \widetilde{r}_k^* \frac{\widetilde{r}_k^{(\ell)}}{|\widetilde{r}_k^{(\ell)}|} \right\} \tag{54}$$

where $\lambda_0 = 0$. Consequently, the optimization problem is

$$\min_{\widetilde{\mathbf{w}}} \frac{\sum_{k\neq 0} \left( \tau_k \left| \widetilde{\mathbf{w}}^H \widetilde{\mathbf{J}}_k \widetilde{\mathbf{x}} \right|^2 + \lambda_k \text{Re}\left\{ (\widetilde{\mathbf{w}}^H \widetilde{\mathbf{J}}_k \widetilde{\mathbf{x}})^* \frac{\widetilde{r}_k^{(\ell)}}{|\widetilde{r}_k^{(\ell)}|} \right\} + \gamma_k \right)}{|\widetilde{\mathbf{w}}^H \widetilde{\mathbf{x}}|^2} \tag{55}$$

which is a nonconvex fractional optimization problem. An efficient solution that directly obtains solution of (55), is to sequentially optimize the filter coefficients by using the CD framework which is discussed in the following.

Let $w_d$, $d \in \{1, \ldots, \widetilde{N}\}$ be the only entry variable of vector $\widetilde{\mathbf{w}}$ while other entries are held fixed and stored in vector $\widetilde{\mathbf{w}}_{-d} \triangleq [w_1, \ldots, w_{d-1}, 0, w_{d+1}, \ldots, w_{\widetilde{N}}]^T$. In this case, to simplify the objective function in (55), we rewrite it based on the variable $w_d$ by the following steps. It can be shown that

$$\left( \widetilde{\mathbf{w}}^H \widetilde{\mathbf{J}}_k \widetilde{\mathbf{x}} \right)^* = \kappa_{1k} w_d + \kappa_{2k}. \tag{56}$$

where

$$\kappa_{1k} = \begin{cases} x^*_{\widetilde{N}-(k-d)} & d \leq k < d + \widetilde{N} \\ 0 & \text{otherwise} \end{cases} \tag{57}$$

and

$$\kappa_{2k} = (\widetilde{\mathbf{w}}_{-d} \circledast \widetilde{\mathbf{x}})_k. \tag{58}$$

Thus, by omitting subscripts $k$ for the sake of notational simplicity from $\kappa_{1k}$ and $\kappa_{2k}$, and considering $w_d = \rho_d e^{j\theta_d}$, it would be straightforward to show that,

$$|\widetilde{\mathbf{w}}^H \widetilde{\mathbf{J}}_k \widetilde{\mathbf{x}}|^2 = |\kappa_1|^2 \rho_d^2 + \kappa_1 \kappa_2^* \rho_d e^{j\theta_d} + \kappa_1^* \kappa_2 \rho_d e^{-j\theta_d} + |\kappa_2|^2. \tag{59}$$

Further, we observe that

$$\begin{aligned} &\text{Re}\left\{ (\widetilde{\mathbf{w}}^H \widetilde{\mathbf{J}}_k \widetilde{\mathbf{x}})^* \frac{\widetilde{r}_k^{(\ell)}}{|\widetilde{r}_k^{(\ell)}|} \right\} \\ &= \frac{1}{|\widetilde{r}_k^{(\ell)}|} \text{Re}\left\{ (\kappa_1 \rho_d e^{j\theta_d} + \kappa_2) \widetilde{r}_k^{(\ell)} \right\} \\ &= \frac{1}{2|\widetilde{r}_k^{(\ell)}|} \left( (\kappa_1^* \rho_d e^{-j\theta_d} + \kappa_2^*) \widetilde{r}_k^{(\ell)} + (\kappa_1 \rho_d e^{j\theta_d} + \kappa_2) \widetilde{r}_k^{*(\ell)} \right). \end{aligned} \tag{60}$$

Thus, the nominator in the objective function (55) can be explicitly written based on $w_d$ as,

$$\sum_{k\neq 0} \left( \tau_k \left| \widetilde{\mathbf{w}}^H \widetilde{\mathbf{J}}_k \widetilde{\mathbf{x}} \right|^2 + \lambda_k \text{Re}\left\{ (\widetilde{\mathbf{w}}^H \widetilde{\mathbf{J}}_k \widetilde{\mathbf{x}})^* \frac{\widetilde{r}_k^{(\ell)}}{|\widetilde{r}_k^{(\ell)}|} \right\} + \gamma_k \right)$$
$$= \widetilde{\eta}_1 \rho_d^2 + \widetilde{\eta}_2 \rho_d e^{j\theta_d} + \widetilde{\eta}_3 \rho_d e^{-j\theta_d} + \widetilde{\eta}_4, \tag{61}$$

with

$$\widetilde{\eta}_1 = \sum_{k\neq 0} \tau_k |\kappa_1|^2,$$

$$\widetilde{\eta}_2 = \sum_{k\neq 0} \left\{ \tau_k \kappa_1 \kappa_2^* + \frac{\lambda_k}{2|\widetilde{r}_k^{(\ell)}|} \kappa_1^* \widetilde{r}_k^{(\ell)} \right\},$$

$$\widetilde{\eta}_3 = \widetilde{\eta}_2^*,$$

$$\widetilde{\eta}_4 = \sum_{k\neq 0} \left\{ \tau_k |\kappa_2|^2 + \frac{\lambda_k}{2|\widetilde{r}_k^{(\ell)}|} \left( \kappa_2^* \widetilde{r}_k^{(\ell)} + \kappa_2 \widetilde{r}_k^{*(\ell)} \right) + \gamma_k \right\}. \tag{62}$$

Similarly, it would be easy to show

$$\left( \widetilde{\mathbf{w}}^H \widetilde{\mathbf{x}} \right)^* = \mu_1 w_d + \mu_2, \tag{63}$$

where $\mu_1 = x_d^*$, and $\mu_2 = \widetilde{\mathbf{x}}^H \widetilde{\mathbf{w}}_{-d}$. Consequently,

$$|\widetilde{\mathbf{w}}^H \widetilde{\mathbf{x}}|^2 = \widetilde{\mu}_1 \rho_d^2 + \widetilde{\mu}_2 \rho_d e^{j\theta_d} + \widetilde{\mu}_3 \rho_d e^{-j\theta_d} + \widetilde{\mu}_4, \tag{64}$$

where

$$\widetilde{\mu}_1 = |\mu_1|^2, \tag{65}$$

$$\widetilde{\mu}_2 = \mu_1 \mu_2^*, \tag{66}$$

$$\widetilde{\mu}_3 = \widetilde{\mu}_2^*, \tag{67}$$

$$\widetilde{\mu}_4 = |\mu_2|^2. \tag{68}$$

Thus, with respect to $\rho_d$ and $\theta_d$, the optimization problem is

$$\mathcal{P}_{\rho_d, \theta_d} \begin{cases} \underset{\rho_d, \theta_d}{\text{minimize}} & f(\rho_d, \theta_d) \\ \text{subject to} & \rho_d \in \mathbb{R} \\ & \theta_d \in [0, 2\pi) \end{cases} \tag{69}$$

where, $f(\rho_d, \theta_d) \triangleq \frac{f_1(\rho_d, \theta_d)}{f_2(\rho_d, \theta_d)}$, and,

$$\begin{aligned} f_1(\rho_d, \theta_d) &\triangleq \widetilde{\eta}_1 \rho_d^2 + \widetilde{\eta}_2 \rho_d e^{j\theta_d} + \widetilde{\eta}_3 \rho_d e^{-j\theta_d} + \widetilde{\eta}_4, \\ f_2(\rho_d, \theta_d) &\triangleq \widetilde{\mu}_1 \rho_d^2 + \widetilde{\mu}_2 \rho_d e^{j\theta_d} + \widetilde{\mu}_3 \rho_d e^{-j\theta_d} + \widetilde{\mu}_4. \end{aligned} \tag{70}$$

Note that $\widetilde{\eta}_1$, $\widetilde{\eta}_4$, $\widetilde{\mu}_1$ and $\widetilde{\mu}_4$ are real values. On the other hands $\widetilde{\eta}_2$ with $\widetilde{\eta}_3$ and $\widetilde{\mu}_2$ with $\widetilde{\mu}_3$ are complex conjugate variables, therefore we encounter with a real function. To design $\theta_d$, and $\rho_d$, one possible solution is to alternatively solve $\mathcal{P}_{\rho_d, \theta_d}$, where we first optimize for $\theta_d$ keeping $\rho_d$ fixed and vice-versa.

In this case, the optimal $\theta_d^\star$ can be calculated by finding real roots of the first order derivative of the objective function and evaluating the objective value in these points and the boundaries. In this regards the derivative of $f(\rho_d, \theta_d)$ with respect to $\theta_d$ can be written as,

$$\frac{\partial f(\rho_d, \theta_d)}{\partial \theta_d} = \frac{\frac{\partial f_1(\rho_d, \theta_d)}{\partial \theta_d} f_2(\rho_d, \theta_d) - \frac{\partial f_2(\rho_d, \theta_d)}{\partial \theta_d} f_1(\rho_d, \theta_d)}{f_2^2(\rho_d, \theta_d)}. \tag{71}$$

From (70) it can be easily shown that,

$$\frac{\partial f_1(\rho_d, \theta_d)}{\partial \theta_d} = j(\widetilde{\eta}_2 \rho_d e^{j\theta_d} - \widetilde{\eta}_3 \rho_d e^{-j\theta_d}),$$
$$\frac{\partial f_2(\rho_d, \theta_d)}{\partial \theta_d} = j(\widetilde{\mu}_2 \rho_d e^{j\theta_d} - \widetilde{\mu}_3 \rho_d e^{-j\theta_d}). \quad (72)$$

Substituting (70) and (72) in (71) and after straight-forward mathematical manipulations, it can be shown that,

$$\frac{\partial f(\rho_d, \theta_d)}{\partial \theta_d} = \frac{e^{-j\theta}(v_2 e^{j2\theta} + v_1 e^{j\theta} + v_0)}{f_2^2(\rho_d, \theta_d)} \quad (73)$$

where,

$$v_2 \triangleq j\rho_d((\widetilde{\eta}_2 \widetilde{\mu}_1 - \widetilde{\eta}_1 \widetilde{\mu}_2)\rho_d^2 + \widetilde{\eta}_2 \widetilde{\mu}_1 - \widetilde{\eta}_1 \widetilde{\mu}_2))$$
$$v_1 \triangleq v_2^* \quad (74)$$
$$v_0 \triangleq j2\rho_d^2(\widetilde{\eta}_2 \widetilde{\mu}_3 - \widetilde{\eta}_3 \widetilde{\mu}_2)\rho_d^2)$$

Using the slack variable $z \triangleq e^{j\theta}$, the critical points can be achieved by obtaining the roots of second degree polynomial of $v_2 z^2 + v_1 z + v_0 = 0$. Let us assume that $z_1$ and $z_2$ be the roots of the aforementioned polynomial function. Therefore the extremum point of $f(\rho_d, \theta_d)$ with respect to $\theta_d$ is $\theta_{1,2} \triangleq -j \ln(z_{1,2})$ and subsequently the optimized phase is,

$$\theta_d^\star = \arg\min_\theta \{f(\rho_d, \theta) \,|\, \theta \in \theta_{1,2}\}. \quad (75)$$

Kindly note that since $f(\rho_d, \theta_d)$ depends on $\sin(\theta_d)$ and $\cos(\theta_d)$; since these are periodic in $[0, 2\pi)$, the objective function also is periodic. Thus, because of the periodicity, we can choose the principal angles as $\theta_d^\star$.

Similar to $\theta_d$, the optimal $\rho_d^\star$ can be calculated by finding real roots of the first order derivative of the objective function with respect to $\theta_d$ and evaluating the objective value in these points and the boundaries. Updating the phase with optimum solution ($\theta_d = \theta_d^\star$) we have,

$$\frac{\partial f(\rho_d, \theta_d^\star)}{\partial \rho_d} = \frac{\frac{\partial f_1(\rho_d, \theta_d^\star)}{\partial \rho_d} f_2(\rho_d, \theta_d^\star) - \frac{\partial f_2(\rho_d, \theta_d^\star)}{\partial \rho_d} f_1(\rho_d, \theta_d^\star)}{f_2^2(\rho_d, \theta_d^\star)} \quad (76)$$

From (70) it can be easily shown that,

$$\frac{\partial f_1(\rho_d, \theta_d^\star)}{\partial \rho_d} = 2\widetilde{\eta}_1 \rho_d + \widetilde{\eta}_2 e^{j\theta_d^\star} + \widetilde{\eta}_3 e^{-j\theta_d^\star},$$
$$\frac{\partial f_2(\rho_d, \theta_d^\star)}{\partial \rho_d} = 2\widetilde{\mu}_1 \rho_d + \widetilde{\mu}_2 e^{j\theta_d^\star} + \widetilde{\mu}_3 e^{-j\theta_d^\star}. \quad (77)$$

Substituting (70) and (77) to (76) and do some mathematical manipulation it can be shown that,

$$\frac{\partial f(\rho_d, \theta_d^\star)}{\partial \rho_d} = \frac{u_2 \rho_d^2 + u_1 \rho_d + u_0}{f_2^2(\rho_d, \theta_d^\star)} \quad (78)$$

where,

$$u_2 \triangleq (\widetilde{\eta}_1 \widetilde{\mu}_2 - \widetilde{\eta}_2 \widetilde{\mu}_1)e^{j\theta_d^\star} + (\widetilde{\eta}_1 \widetilde{\mu}_3 - \widetilde{\eta}_3 \widetilde{\mu}_1)e^{-j\theta_d^\star}$$
$$u_1 \triangleq 2(\widetilde{\eta}_1 \widetilde{\mu}_4 - \widetilde{\eta}_4 \widetilde{\mu}_1) \quad (79)$$
$$u_0 \triangleq (\widetilde{\eta}_2 \widetilde{\mu}_4 - \widetilde{\eta}_4 \widetilde{\mu}_2)e^{j\theta_d^\star} + (\widetilde{\eta}_3 \widetilde{\mu}_4 - \widetilde{\eta}_4 \widetilde{\mu}_3)e^{-j\theta_d^\star}$$

The extremum points with respect to $\rho_d$ can be obtain by calculating the roots of the following second degree polynomial function, $u_2 \rho_d^2 + u_1 \rho_d + u_0 = 0$. Let $\rho_1$ and $\rho_2$ be the roots of the aforementioned polynomial function. Since $0$ is the lower bound of $\rho_d$ ($\rho_d \geq 0$), another critical point of the objective function with respect to $\rho_d$ is $\rho_3 = 0$. Therefore in total the critical points of $f(\rho_d, \theta_d^\star)$ with respect to $\rho_d$ are $\{\rho_1, \rho_2, \rho_3\}$. Subsequently the optimized amplitude is,

$$\rho_d^\star = \arg\min_\rho \{f(\rho, \theta_d^\star) \,|\, \rho \in \rho_{1,2,3}\}. \quad (80)$$

Please note that, since $\rho_3 = 0$ is one of the critical points, therefore we have at least one solution for $\rho_d$ and the optimization become not infeasible.

Once $\rho_d^\star$ is obtained, $\widetilde{w}$ will be updated by $w_d^\star = \rho_d^\star e^{j\theta_d^\star}$.

*Remark 4.1:* For the special case $p = 2$, it would be straightforward to show that the optimization problem can be cast to the form of (25), with $\mathbf{R} = \sum_{k=1}^{\widetilde{N}} \mathbf{J}_k \mathbf{x} \mathbf{x}^H \mathbf{J}_k^H$. In this case, MVDR can directly find the optimal $\widetilde{w}^\star = \mathbf{R}^{-1}\mathbf{x}$.

### B. Optimization of waveform

For a fixed $\widetilde{w}$, the optimization problem is

$$\mathcal{P}_{\widetilde{x}} \begin{cases} \underset{\widetilde{x}}{\text{minimize}} & \displaystyle\sum_{\substack{k=-\widetilde{N}+1 \\ k \neq 0}}^{\widetilde{N}-1} \frac{|\widetilde{w}^H \widetilde{\mathbf{J}}_k \widetilde{x}|^p}{|\widetilde{w}^H \widetilde{x}|^2} \\ \text{subject to} & \mathbf{x} \in \Omega_h \end{cases} \quad (81)$$

we note that the problem in (81) is a special case of (44) under $\Omega_\infty$, and its solution can be achieved by using procedures identical to those used to find $\theta_d^\star$. As a result, only the solution to (81) under the constraint of a discrete phase waveform, namely $\Omega_L$, is provided in this section. In this instance, the problem can be solved immediately as shown in the details below using the CD framework and fast Fourier transform (FFT) operator.

Let $x_d = e^{j\phi_d}$, $d \in \{1, \ldots, N\}$ be the only entry variable of vector $\mathbf{x}$ while other entries are held fixed and stored in vector $\mathbf{x}_{-d} \triangleq [x_1, \ldots, x_{d-1}, 0, x_{d+1}, \ldots, x_N]^T$, and $\widetilde{x}_{-d} = [\mathbf{0}_M^T, \mathbf{x}_{-d}^T, \mathbf{0}_M^T]^T$. Then,

$$|\widetilde{w}^H \widetilde{\mathbf{J}}_k \widetilde{x}|^p = |a_{1k} e^{j\phi_d} + a_{2k}|^p \quad (82)$$

where

$$a_{1k} = \begin{cases} w_{\widetilde{N}-(k-d)}^* & d \leq k < d + \widetilde{N} \\ 0 & \text{otherwise} \end{cases} \quad (83)$$

and

$$a_{2k} = (\widetilde{x}_{-d} \circledast \widetilde{w})_k. \quad (84)$$

Also,

$$|\widetilde{w}^H \widetilde{x}|^2 = |b_1 e^{j\phi_d} + b_2|^2, \quad (85)$$

where $b_1 = w_d^*$, and $b_2 = \widetilde{w}^H \widetilde{x}_{-d}$. In this case, the optimization problem with respect to the phase variable $\phi_d$

by removing the constant terms is

$$
\mathcal{P}_{\phi_d}
\begin{cases}
\min_{\phi_d} & \sum_{\substack{k=-\widetilde{N}+1 \\ k \neq 0}}^{\widetilde{N}-1} \dfrac{|a_{1k}e^{j\phi_d} + a_{2k}|^p}{|b_1 e^{j\phi_d} + b_2|^2} \\
s.t. & \phi_d \in \{1, e^{j\frac{2\pi}{L}}, \ldots, e^{j\frac{2\pi(L-1)}{L}}\}
\end{cases}
\tag{86}
$$

Note that in the optimization problem (86), all the discrete points lie on the boundary of the optimization problem; hence, all of them are critical points for the problem. Interestingly, the solution to the aforementioned problem can be obtained efficiently using an FFT operation due to the fact that the objective function represents the modulus of the $L$-point discrete Fourier transform (DFT) of a sequence associated with coefficients $a_{1k}$, $a_{2k}$, $b_1$, and $b_2$. Precisely, we find the index $l^\star$ by

$$
l^\star = \arg \min_{l=1,\ldots,L} \sum_{\substack{k=-\widetilde{N}+1 \\ k \neq 0}}^{\widetilde{N}-1} \frac{|\mathcal{F}_L\{a_{1k}, a_{2k}\}|^p}{|\mathcal{F}_L\{b_1, b_2\}|^2}, \tag{87}
$$

where $\mathcal{F}_L$ indicates $L$-point FFT operation. Hence, $\phi_d^\star = \frac{2\pi(l^\star-1)}{L}$ and $x_d^\star = e^{j\phi_d^\star}$.

The summary of the proposed method is given by **Algorithm 2**, where, $\widetilde{\mathbf{x}}^\star$ and $\widetilde{\mathbf{w}}^\star$ are the optimized solution. To obtain this solution, the algorithm considers an initial waveform $\widetilde{\mathbf{x}}^{(0)}$ and its corresponding matched filter coefficient $\widetilde{\mathbf{w}}^{(0)} = (\widetilde{\mathbf{x}}^{(0)})^H$ as the initial filter. Then, at each iteration, it alternates between solving the problems of $\mathcal{P}_{\widetilde{\mathbf{w}}}$ and $\mathcal{P}_{\widetilde{\mathbf{x}}}$. This procedure is repeated until all the algorithm examines the convergence metric for the objective function.

---

**Algorithm 2** CD - ISL/PSL-based Joint Waveform and Mismatch Filter Design

---

**Input:** value of $p$, initial waveform, and filter coefficients
**Output:** $\widetilde{\mathbf{x}}^\star, \widetilde{\mathbf{w}}^\star$

1: set $n \leftarrow 0$
2: **repeat**
3:      set $d \leftarrow 1$
4:      **repeat**
5:          Find $\rho_d^\star$ by solving $\mathcal{P}_{\rho_d}$;
6:          Find $\theta_d^\star$ by solving $\mathcal{P}_{\theta_d}$;
7:          $w_d^\star = \rho_d^\star e^{j\theta_d^\star}$;
8:          $d \leftarrow d + 1$
9:      **until** $d = \widetilde{N}$
10:     set $d \leftarrow 1$
11:     **repeat**
12:         $l^\star = \arg\min_{l=1,\ldots,L} \sum_{\substack{k=-\widetilde{N}+1 \\ k \neq 0}}^{\widetilde{N}-1} \frac{|\mathcal{F}_L\{a_{1k}, a_{2k}\}|^p}{|\mathcal{F}_L\{b_1, b_2\}|^2}$;
13:         $\phi_d^\star = \frac{2\pi(l^\star-1)}{L}$;
14:         $x_d^\star = e^{j\phi_d^\star}$;
15:         $d \leftarrow d + 1$
16:     **until** $d = N$
17:     $n \leftarrow n + 1$
18: **until** convergence

---

## V. NUMERICAL EXAMPLES

In this section, we show through numerical examples how to effectively employ the pulse compression methodology in a weather radar system using the suggested optimized waveforms, and the related receive filter. In order to achieve this, we first evaluate the performance of the proposed algorithms in terms of convergence behavior and the quality of the solutions. We then evaluate the results on real weather radar time series ($I$ and $Q$), by analyzing the reflectivity, spectrum width, correlation coefficient, and differential phase[2].

### A. Convergence Behaviour and Autocorrelation Sidelobes

Figure 1 illustrates the convergence behaviour and autocorrelation functions of the waveforms obtained by algorithms 1 and 2, which are herein referred to as ADMM and CD, respectively. We set $N = 64$ and $M = 128$ (i.e., the filter length $\widetilde{N} = 2 \times M + N = 320$), and run the algorithms for 1000 iterations to obtain the convergence curve shown in this figure. The initial sequence for the curves in this figure was a random polyphase code, and that was identically used for both ADMM and CD methods. For ADMM, we use $\rho_1 = 16$, $\rho_2 = 40$; and for CD, we show the results for the cases $p = 2$, and $p = 6$. Additionally, the two design algorithms are constrained to constant modulus codes, such that the resultant waveforms would not cause performance degradation due to a potential distortion from transmit power amplifier nonlinearity.

Despite the fact that CD and ADMM used different objective functions in this study, Figure 1a shows a monotonic decrement of the objective value with regards to the number of iterations. We explicitly solve the problem (20) using the ADMM approach, but (43) using the CD method, which alters the objective function based on the value of $p$ chosen. Figure 1b demonstrates small correlation levels for the optimized sequences by both ADMM and CD approaches. The areas outside of the highlighted area display the correlation function's extension area, which is related to the receive filter length, that is considered to be longer than the sequence length in this study. Note that, in the event when $p = 6$, CD obtains a flat correlation level for the sidelobes, that is due to the mismatch PSL minimization. Additionally, CD with $p = 2$ has acquired extremely low correlation sidelobe values. As a benchmark, the autocorrelation functions of the method reported in [53] and [25], which are referred to as CAN and Gradient Descent, respectively, together with the autocorrelation function of the initial sequence are also shown in this figure. For the Gradient Descent technique [25], we gradually increase the $p$ values from 2 to $2^2$, $2^3$, $2^4$, and $2^6$ as suggested in [28] to obtain very small values in PSL. We also choose a certain amount of lags to be minimized for the Gradient Descent technique, so that the extra degree of freedom offers a very low sidelobe level in an area near the main peak of objects. This is critical for weather applications because sidelobes can introduce uncertainty into reflectivity calculations. We precisely adjust the weight factor to one for

---

[2]We omit the effects of alphabet size ($L$) in the numerical results without sacrificing generality and use the case where the alphabet size is not limited.
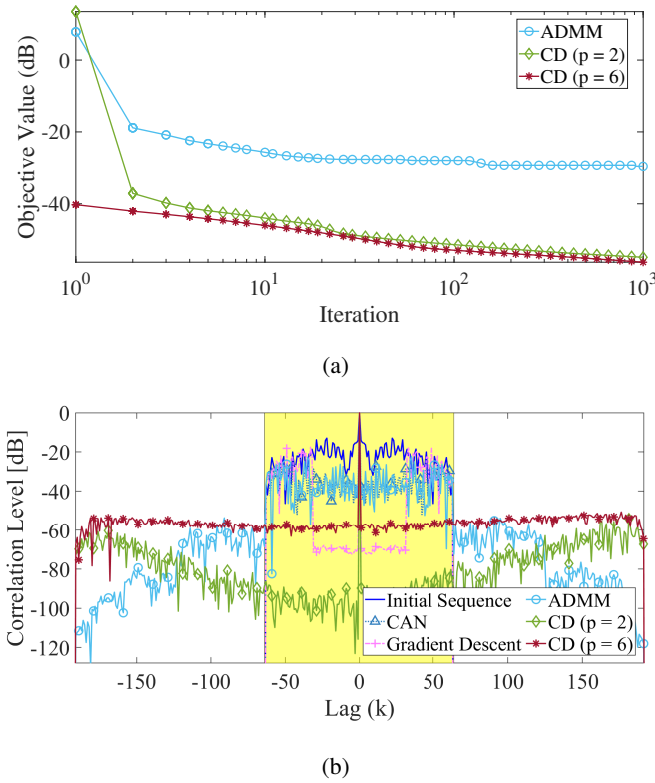
(a)



(b)

Figure 1: (a) Convergence behavior of the proposed algorithms 1 and 2 and (b) Autocorrelation functions of the waveforms obtained by algorithms 1 and 2, with 200 iterations for $N = 64$ and $M = 128$. The autocorrelation function of the initial sequence and an optimized sequence that is obtained.

the 62 lags around the main peak of the autocorrelation and keep the weight at zero for the remainder of the Gradient Descent method.

### B. Reflectivity Estimation Error

The dynamic range of precipitation reflectivity in weather radar applications is relatively high, sometimes surpassing 55 dBZ [74]. In this case, the calculation of the reflectivity value will be distorted by waveforms that do not have extremely low correlation sidelobes after pulse compression. In order to demonstrate this influence on the designed waveform, we consider a weather radar with maximum range of 30 km and range resolution 31.25 m. We convolve each of the optimized waveforms from the earlier categories of ADMM, CD ($p = 2$), CD ($p = 6$), CAN, and Gradient Descent with a signal containing mask, which is built with certain reflectivity values that must be estimated after pulse compression. Then, we convolve the obtained uncompressed samples with the optimized filter coefficients. The results, which are displayed in Figure 2, reveal that only CD ($p = 2$) was able to closely match the mask. As to the mask, we consider three range

intervals[3] of 4 km to 7 km, 7.003 km to 14 km, and 14.003 km to 25 km, with three distinct reflectivity values[4] levels of 25 dBZ, 40 dBZ, and 10 dBZ, respectively. Figure 2a shows how the jumps between the reflectivity levels in this simulated environment have had a substantial impact on the estimated level of the reflectivity, emphasizing the necessity of simultaneous waveform and filter optimization for avoiding this effect.

To demonstrate the impact of pulse compression on the Doppler domain, we also take into account a second pulse that was returned from the simulated scene with a similar reflectivity in the amplitude but a different phase value in every region. Accordingly, the regions one, two, and three have phase differences of $-\frac{\pi}{12}$, $\frac{\pi}{6}$, and $0$ radian, respectively. Figure 2b demonstrates that waveform correlation sidelobes can have an adverse effect not only on the reflectivity levels, but also on the phase of the reflectivity as well. Note that the phase evaluation is only valid in the highlighted area; elsewhere, noise affects the phase, where there is no signal reflection in the simulation.

### C. Blind Range Suppression

Figure 3 illustrates the use of partial correlation to reduce blind range for a waveform with length $N = 289$ that results in 9.0313 km of blind range in a radar with range resolution 31.25m. The reflectivity inside the blind range can be partially identified when employing partial correlation with CD or CAN techniques. However, CD with optimized waveform and filter follows more precisely the mask as indicated in this figure. For this figure, the initial waveform for both CD and CAN is the Px code [75], and the mismatch filter length was kept identical to the code length ($M = 0$). Note that the gain-loss for the partially decoded signal is calculated by comparing the amplitude of the partially decoded signal to that of the full decoded signal. The resulting value is used as a calibration factor and applied to the partially decoded signal (more details for gain-loss calibration can be found in [15]).

### D. Real Data

In this section, we evaluate the effectiveness of the enhanced waveform and subpulse-filter combinations by analyzing real-world weather data from ELDES (https://www.eldesradar.com/). The data was collected during a period of heavy rainfall in Florence, Italy, on September 30, 2022. The principle radar's specifications are listed in TABLE I, and further information about it can be found in [76]. The collected $I$ and $Q$ data are obtained from an uncoded pulse with a resolution 31.25m. In order to replicate the effects of pulse compression on these observations, we convolve the optimized waveform (designed in the previous section) with the echoes captured by the radar when transmitting an uncoded pulse. The acquired uncompressed samples are then convolved with

---

[3]The initial range interval and the issue with the blind range of the pulse-compression radars is covered in the following section.

[4]The reflectivity $Z$ (in units of $mm^6/m^3$) commonly span many orders of magnitude, and hence a logarithmic scale $\text{dB}Z = 10 \log_{10} Z$ is used.

TABLE I: Technical Specifications of the weather radar used for recording $I$ and $Q$ data.

| Specification: | Value |
|---|---|
| Type: | Dual Polarized Weather Radar System |
| Operating frequency: | 9410MHz ±30MHz |
| Peak power: | 25Kw (12.5Kw Horizontal Channel - 12.5Kw Vertical Channel) |
| Pulse width: | 0.2 - 0.4 - 0.8$\mu s$ (typ.) User selectable |
| Repetition frequency (PRF): | $1000 - 800 - 500$ Hz User selectable |
| Receiver: | Linear Digital for simultaneous dual-polarization coherent on receive (Doppler) |
| Transmitter: | Magnetron |
| Dynamic range: | $> 90$dB |
| Antenna Type: | Parabolic prime focus reflector |
| Horizontal and Vertical Beamwidth: | $\leq 2, 5$ deg |
| Gain: | $\geq 36$ dB |
| Range scale: | 30Km - 40Km - 60Km - 120Km User selectable |
| Range resolution: | 31.25m, 62.5m, 125m |
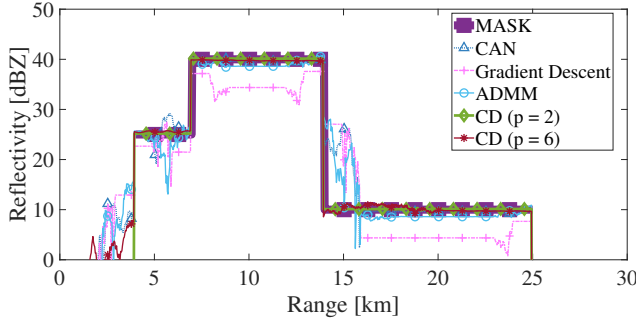


(a)
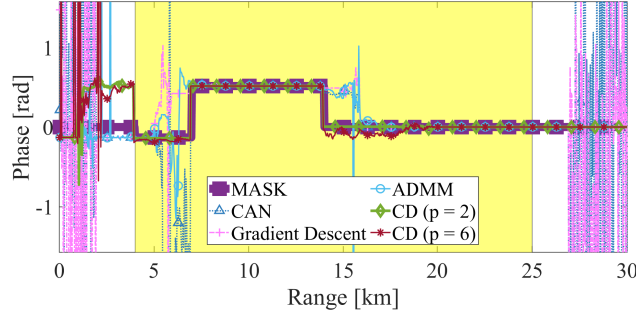


(b)

Figure 2: Reflectivity level estimation by performing pulse compression based on ADMM, CD ($p = 2$), CD ($p = 6$), CAN, and Gradient Descent waveforms. (a) Reflectivity levels. (b) Phase. The figure shows only CD ($p = 2$) due to very low correlation sidelobes is able to closely match the mask.
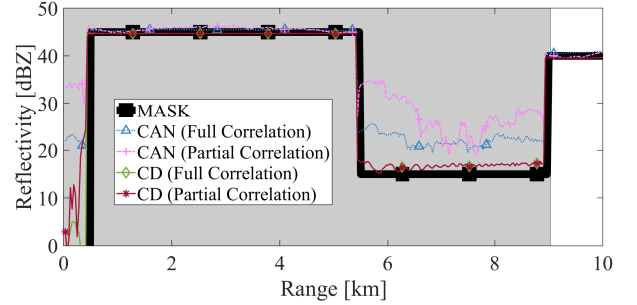


Figure 3: Application of partial correlation for reducing a pulse compression radar's blind range. The gray background indicates the area that is blind to radar because the receiver is turned off during the transmission. The full correlation demonstrates the assumption that the receiver was turned on during the transmission time, allowing for the capture of all reflections. Partial correlation indicates the possibility of identifying the reflection in the blind range, given that some reflections are received after the gray area when the receiver is turned on.

the optimized filter coefficients[5]. Therefore, we assess the effectiveness of the optimized waveform and subpluse-filter pair using real data from the aforementioned system.

In Figure 4, we present the analysis of horizontal reflectivity

[5]The code length $N = 64$, filter length $\widetilde{N} = 320$, and all the other algorithm parameters are identical to those used in the first part of the numerical results.

values obtained from the dataset "IQP2227223270U.003". The results clearly indicate that each of the described methods introduces deviations from the benchmark reflectivity image. These deviations manifest as artifacts that appear in different regions of the image. When partial correlation is applied in the blind range region, these artifacts become more pronounced. This is due to the nature of partial correlation, which can introduce additional distortions and inconsistencies in the reflectivity image. To mitigate these artifacts, one possible approach is to use an uncoded short pulse specifically designed for the blind range, while employing a long coded pulse for the remaining ranges. This combination can help reduce the impact of artifacts in the blind range region. However, it's important to note that even when utilizing a long coded pulse, the range sidelobes of the pulse and the receive filter can still contribute to the generation of artifacts. These artifacts arise from the side effects of the pulse compression process and the characteristics of the receive filter. To minimize these artifacts, it is crucial to select a waveform and filter pair that exhibit

smaller correlation sidelobes. Among the methods analyzed in this paper, CD ($p = 2$) demonstrates a closer match to the benchmark reflectivity values. This indicates that CD ($p = 2$) has waveform and filter characteristics that result in smaller correlation sidelobes, leading to a reduction in artifacts and a more faithful representation of the reflectivity image.

To support this observation, we calculate the difference between the reflectivity values of each image and the benchmark for the entire available dataset. The norm of this difference was used as the MSE of the method for both horizontal and vertical polarization, as shown in Tables II and III, respectively. The results clearly demonstrate that CD with $p = 2$ consistently exhibits the lowest MSE, indicating that the proposed methodology can effectively produce reflectivity values that closely match the benchmark.

Based on the results of the experiment on real data, one can conclude that mismatched ISL is the most reliable or robust metric for designing waveform and filter pairs in weather radar applications. The CD technique exhibits superior performance compared to other methods, particularly in terms of mismatched ISL, which could be the reason for its excellent results, even inside of the blind range. This observation can be investigated further by calculating the phase shift in the returned signal, which is related to the wind velocity using pulse pair processing. Note that the phase of the backscattered signal received at the radar varies significantly from pulse to pulse due to the individual drop returns. However, the mean Doppler shift provides a precise indication of the radial velocity inside the weather sample volume if a sufficient number of returns are integrated (typically several pulses). The radial velocity for the benchmark, CAN, GD, and the proposed methods is depicted in Figure 5. When the obtained results are compared to the benchmark, it is clear that the proposed methods can estimate precisely the radial velocity. However, depending on the method used, there may be some deviations from the actual values. To verify this behavior, we have included an example of the angle cut at 7.0807 degrees for the reflectivity and radial velocity plots in Figure 4 and Figure 5, respectively. These angle cut plots can be found in Figure 6. Upon observing this figure, it is evident that CD ($p = 2$) provides the best match with the benchmark in both reflectivity and radial velocity values. However, ranking the other approaches is more challenging, as it is also reflected in Tables II and III. Additionally, note that Tables II and III present average metrics for each dataset, while Figure6 offers angle cuts, providing a more detailed perspective on the performance.

### E. Polarimetric Variables

In addition to reflectivity and Doppler, two other parameters related to weather sensing include the differential phase and the correlation coefficient. The differential propagation phase, $\phi_{DP}$, is defined as the phase difference between horizontally and vertically polarized signals, and can be expressed as:

$$\phi_{DP} = \angle \langle S_h S_v^* \rangle \tag{88}$$

where $S_\mathrm{h}$ and $S_\mathrm{v}$ are the complex amplitudes of the horizontally and vertically polarized signals, respectively. The values of $\phi_{DP}$ reveal information about the nature of the scatterers being sampled. Correlation coefficient (also referred to as $\rho_{hv}$ or $\rho$) provides a measure of the consistency of the shapes and sizes of drops within the radar beam[6], and can be expressed as:

$$\rho_{hv} = \frac{|\langle S_h S_v^* \rangle|}{\sqrt{\langle |S_h|^2 \rangle \langle |S_v|^2 \rangle}}. \tag{89}$$

where $\langle \cdot \rangle$ denotes averaging over the radar pulse volume. A higher value of correlation coefficient shows a higher consistency in the size and shape of drops, while a lower value indicates greater variability in shapes and sizes. The correlation coefficient can further help for distinguishing between meteorological and non-meteorological objects, finding the melting layer, identifying giant hail, exploring tornadic debris, and checking the quality of other dual polarization products.

The differential phase and the correlation coefficient are dependent on the transmit waveform and receive filters; though not optimized directly, the following example shows effects of pulse compression on estimating these parameters. Figure 7 and Figure 8 indicate respectively $\phi_{DP}$ and $\rho_{hv}$ of the returned signal for the benchmark and generated data using pulse compression via CAN, GD, and the proposed methods, respectively. These figures show that the radar moment estimation using the optimized waveform and filter pair obtained by CD ($p = 2$) is close to the benchmark differential phase and correlation coefficient, indicating that the optimized subpulse-filter pairs are of high quality in weather radar applications.

### VI. CONCLUSION

For the purpose of implementing a successful pulse compression on weather radar, we proposed an optimization-based method. Through the proposed method, the transmitted codes and the extended filter are jointly designed, which guarantees that the pulse compression will possess a low sidelobe level and further a better estimation of the meteorological reflectivity. The results obtained through real data demonstrate the efficacy of the proposed approach and the improvement brought by this well-designed pulse compression technique. Despite the fact that ADMM successfully reduces MSE, the CD-based range sidelobe optimization actually performs better in real-weather radar applications. Future research may explore the development of waveforms that are optimized for both full and partial correlation sidelobe levels.

---

[6]The correlation coefficient $\rho$ is a dimensionless quantity that provides a measure of the degree of correlation between the horizontal and vertical polarizations of the radar signal.
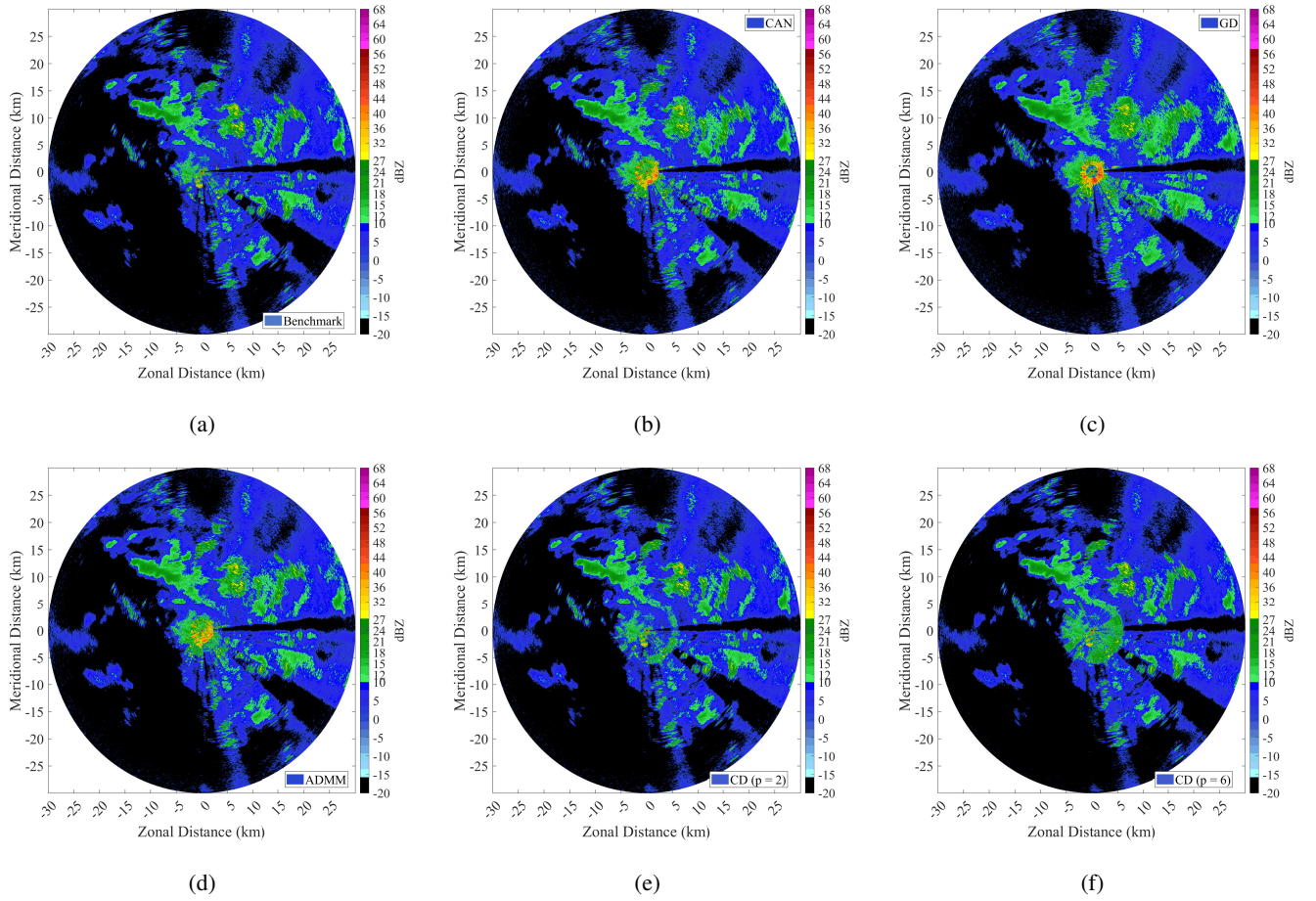
(a)  (b)  (c)

(d)  (e)  (f)

Figure 4: Assessing the utility of the optimized waveform and subpluse-filter pair based on horizontal reflectivity of real data from ELDES; (a) indicates reflectivity (dBZ) of real weather data as the benchmark that was recorded on September 30, 2022, in Florence, Italy, during a time of rain. The remaining images represent the impact of applying pulse compression to real data reflectivity (dBZ) using (b) CAN, (c) Gradient Descent, (d) ADMM , (e) CD ($p = 2$), and (f) CD ($p = 6$).

## REFERENCES

[1] L. Wu, M. Alaee-Kerahroodi, and B. M. R. Shankar, "Improving pulse-compression weather radar via the joint design of subpulses and extended mismatch filter," in *IGARSS 2022 - 2022 IEEE International Geoscience and Remote Sensing Symposium*, 2022, pp. 469–472.

[2] C. E. Cook, "Pulse compression-key to more efficient radar transmission," *Proceedings of the IRE*, vol. 48, no. 3, pp. 310–316, 1960.

[3] E. Fowle, "The design of fm pulse compression signals," *IEEE Transactions on Information Theory*, vol. 10, no. 1, pp. 61–67, 1964.

[4] J. Kroszczynski, "Pulse compression by means of linear-period modulation," *Proceedings of the IEEE*, vol. 57, no. 7, pp. 1260–1266, 1969.

[5] S. Blunt and K. Gerlach, "Adaptive pulse compression via MMSE estimation," *IEEE Transactions on Aerospace and Electronic Systems*, vol. 42, no. 2, pp. 572–584, 2006.

[6] M. Alaee-Kerahroodi, P. Babu, M. Soltanalian, and M. B. Shankar, *Signal Design for Modern Radar Systems*. Artech House, 2022.

[7] A. Kostic, D. Milovanovic, P. Vukovic, P. Eferica, and D. Rancic, "An improved weather radar signal processing algorithm implemented on mitsubishi rc-34a radar," in *4th International Conference on Telecom-munications in Modern Satellite, Cable and Broadcasting Services. TELSIKS'99 (Cat. No.99EX365)*, vol. 2, 1999, pp. 349–354 vol.2.

[8] B. L. Cheong, R. Kelley, R. D. Palmer, Y. Zhang, M. Yeary, and T.-Y. Yu, "Px-1000: A solid-state polarimetric X-band weather radar and time–frequency multiplexed waveform for blind range mitigation," *IEEE Transactions on Instrumentation and Measurement*, vol. 62, no. 11, pp. 3064–3072, 2013.

[9] D. Schvartzman and S. Torres, "Design of practical pulse compression waveforms for polarimetric phased array radar," in *Proc. 39th Int. Conf. Radar Meteorol.*, 2019, pp. 1–9.

[10] A. Mudukutore, V. Chandrasekar, and R. Keeler, "Pulse compression for weather radars," *IEEE Transactions on Geoscience and Remote Sensing*, vol. 36, no. 1, pp. 125–142, 1998.

[11] R. M. Beauchamp, S. Tanelli, E. Peral, and V. Chandrasekar, "Pulse compression waveform and filter optimization for spaceborne cloud and precipitation radar," *IEEE Transactions on Geoscience and Remote Sensing*, vol. 55, no. 2, pp. 915–931, 2017.

[12] J. Wang, E. Brookner, and M. Gerecke, "Analysis of concatenated waveforms and required stc," in *2008 IEEE Radar Conference*, 2008, pp. 1–6.

[13] N. Bharadwaj, K. V. Mishra, and V. Chandrasekar, "Waveform con-

TABLE II: MSE of the horizontal reflectivity values for different filter and waveform pairs.

| Data Set | MSE | | | | |
|---|---|---|---|---|---|
| | CAN | Gradient Descent | ADMM | CD (p = 2) | CD (p = 6) |
| IQP2227223270U.001 | 3.1412016e+04 | 3.3911836e+04 | 3.3963066e+04 | 2.1481277e+04 | 3.7338535e+04 |
| IQP2227223270U.002 | 2.4120281e+04 | 2.7934445e+04 | 2.4007596e+04 | 1.4239896e+04 | 2.3550652e+04 |
| IQP2227223270U.003 | 1.6463525e+04 | 2.0161645e+04 | 1.6361785e+04 | 7.6400356e+03 | 1.2583212e+04 |
| IQP2227223300U.001 | 3.0578844e+04 | 3.3001906e+04 | 3.2862273e+04 | 2.2064354e+04 | 3.7281277e+04 |
| IQP2227223300U.002 | 2.3392654e+04 | 2.7282885e+04 | 2.3301863e+04 | 1.5958033e+04 | 2.5144506e+04 |
| IQP2227223300U.003 | 1.5875740e+04 | 1.9590947e+04 | 1.5734106e+04 | 9.5832852e+03 | 1.5772477e+04 |
| IQP2227223330U.001 | 3.1096500e+04 | 3.3636680e+04 | 3.3354984e+04 | 2.2584271e+04 | 3.7730293e+04 |
| IQP2227223330U.002 | 2.4538041e+04 | 2.8369082e+04 | 2.4507979e+04 | 1.6620434e+04 | 2.6358029e+04 |
| IQP2227223330U.003 | 1.8285496e+04 | 2.1919756e+04 | 1.8395701e+04 | 1.0061450e+04 | 1.8589279e+04 |

TABLE III: MSE of the vertical reflectivity values for different filter and waveform pairs.

| Data Set | MSE | | | | |
|---|---|---|---|---|---|
| | CAN | Gradient Descent | ADMM | CD (p = 2) | CD (p = 6) |
| IQP2227223270U.001 | 3.1294170e+04 | 3.3931117e+04 | 3.2990730e+04 | 2.3185225e+04 | 3.7202813e+04 |
| IQP2227223270U.002 | 2.4819670e+04 | 2.8343582e+04 | 2.4224777e+04 | 1.5413740e+04 | 2.4035875e+04 |
| IQP2227223270U.003 | 1.7759506e+04 | 2.0870076e+04 | 1.7472773e+04 | 7.0154404e+03 | 1.2071680e+04 |
| IQP2227223300U.001 | 3.0542654e+04 | 3.3236391e+04 | 3.1892439e+04 | 2.3684432e+04 | 3.7465832e+04 |
| IQP2227223300U.002 | 2.4833236e+04 | 2.8306467e+04 | 2.4303291e+04 | 1.6833055e+04 | 2.5494072e+04 |
| IQP2227223300U.003 | 1.7448410e+04 | 2.0554023e+04 | 1.6972426e+04 | 1.0222998e+04 | 1.5561700e+04 |
| IQP2227223330U.001 | 3.1313115e+04 | 3.4026313e+04 | 3.2636525e+04 | 2.4614045e+04 | 3.8187887e+04 |
| IQP2227223330U.002 | 2.6001777e+04 | 2.9471674e+04 | 2.5418355e+04 | 1.7511568e+04 | 2.6646209e+04 |
| IQP2227223330U.003 | 1.9763447e+04 | 2.2951859e+04 | 1.9574166e+04 | 1.1522604e+04 | 1.8888014e+04 |

siderations for dual-polarization doppler weather radar with solid-state transmitters," in *2009 IEEE International Geoscience and Remote Sensing Symposium*, vol. 3, 2009, pp. III–267–III–270.

[14] M. Kumar and V. Chandrasekar, "Intrapulse polyphase coding system for second trip suppression in a weather radar," *IEEE Transactions on Geoscience and Remote Sensing*, vol. 58, no. 6, pp. 3841–3853, 2020.

[15] C. M. S. Aquino, B. Cheong, and R. D. Palmer, "Progressive pulse compression: A novel technique for blind range recovery for solid-state radars," *Journal of Atmospheric and Oceanic Technology*, vol. 38, no. 9, pp. 1599 – 1611, 2021. [Online]. Available: https://journals.ametsoc.org/view/journals/atot/38/9/JTECH-D-20-0164.1.xml

[16] N. Bharadwaj and V. Chandrasekar, "Wideband waveform design principles for solid-state weather radars," *Journal of Atmospheric and Oceanic Technology*, vol. 29, no. 1, pp. 14 – 31, 2012.

[17] J. E. Cilliers and J. C. Smit, "Pulse compression sidelobe reduction by minimization of $l_p$-norms," *IEEE Transactions on Aerospace and Electronic Systems*, vol. 43, no. 3, pp. 1238–1247, 2007.

[18] P. Stoica, J. Li, and M. Xue, "Transmit codes and receive filters for pulse compression radar systems," in *2008 IEEE International Conference on Acoustics, Speech and Signal Processing*, 2008, pp. 3649–3652.

[19] U. Niesen, D. Shah, and G. W. Wornell, "Adaptive alternating minimization algorithms," *IEEE Transactions on Information Theory*, vol. 55, no. 3, pp. 1423–1429, 2009.

[20] A. De Maio, Y. Huang, M. Piezzo, S. Zhang, and A. Farina, "Design of radar receive filters optimized according to $l_p$-norm based criteria," *IEEE Transactions on Signal Processing*, vol. 59, no. 8, pp. 4023–4029, 2011.

[21] O. Rabaste and L. Savy, "Mismatched filter optimization for radar applications using quadratically constrained quadratic programs," *IEEE Transactions on Aerospace and Electronic Systems*, vol. 51, no. 4, pp. 3107–3122, 2015.

[22] P. J. Kajenski, "Mismatch filter design via convex optimization," *IEEE Transactions on Aerospace and Electronic Systems*, vol. 52, no. 4, pp. 1587–1591, 2016.

[23] Y. Jing, J. Liang, S. A. Vorobyov, X. Fan, and D. Zhou, "Efficient joint transmit waveform and receive filter design based on a general lp-norm metric for sidelobe level of pulse compression," *Signal Processing*, vol. 188, p. 108174, 2021.

[24] K. Zhou, S. Quan, D. Li, T. Liu, F. He, and Y. Su, "Waveform and filter joint design method for pulse compression sidelobe reduction," *IEEE Transactions on Geoscience and Remote Sensing*, vol. 60, pp. 1–15, 2022.

[25] J. M. Baden, B. O'Donnell, and L. Schmieder, "Multiobjective sequence design via gradient descent methods," *IEEE Transactions on Aerospace and Electronic Systems*, vol. 54, no. 3, pp. 1237–1252, 2018.

[26] G. Cui, X. Yu, Y. Yang, and L. Kong, "Cognitive phase-only sequence design with desired correlation and stopband properties," *IEEE Transactions on Aerospace and Electronic Systems*, vol. 53, no. 6, pp. 2924–2935, 2017.

[27] G. Galati, G. Pavan, and F. De Palo, "Chirp signals and noisy waveforms for solid-state surveillance radars," *Aerospace*, vol. 4, no. 1, p. 15, Mar 2017. [Online]. Available: http://dx.doi.org/10.3390/aerospace4010015

[28] M. Alaee-Kerahroodi, A. Aubry, A. De Maio, M. M. Naghsh, and M. Modarres-Hashemi, "A coordinate-descent framework to design low PSL/ISL sequences," *IEEE Transactions on Signal Processing*, vol. 65, no. 22, pp. 5942–5956, Nov 2017.

[29] G. Cui, X. Yu, M. Piezzo, and L. Kong, "Constant modulus sequence set design with good correlation properties," *Signal Processing*, vol. 139, pp. 75–85, 2017.

[30] Y. Jing, J. Liang, B. Tang, and J. Li, "Designing unimodular sequence with low peak of sidelobe level of local ambiguity function," *IEEE Transactions on Aerospace and Electronic Systems*, vol. 55, no. 3, pp. 1393–1406, 2019.

[31] A. Thakur, S. R. Talluri, and R. K. Panigrahi, "Side-lobe reduction in pulse compression having a better range resolution," *Computers & Electrical Engineering*, vol. 74, pp. 520–532, 2019. [Online]. Available: https://www.sciencedirect.com/science/article/pii/S0045790617314866

[32] R. Lin, M. Soltanalian, B. Tang, and J. Li, "Efficient design of binary sequences with low autocorrelation sidelobes," *IEEE Transactions on Signal Processing*, vol. 67, no. 24, pp. 6397–6410, 2019.

[33] X. Yu, G. Cui, J. Yang, J. Li, and L. Kong, "Quadratic optimization for unimodular sequence design via an adpm framework," *IEEE Transactions on Signal Processing*, vol. 68, pp. 3619–3634, 2020.

[34] R. Jyothi, P. Babu, and M. Alaee-Kerahroodi, "Slope: A monotonic algorithm to design sequences with good autocorrelation properties by
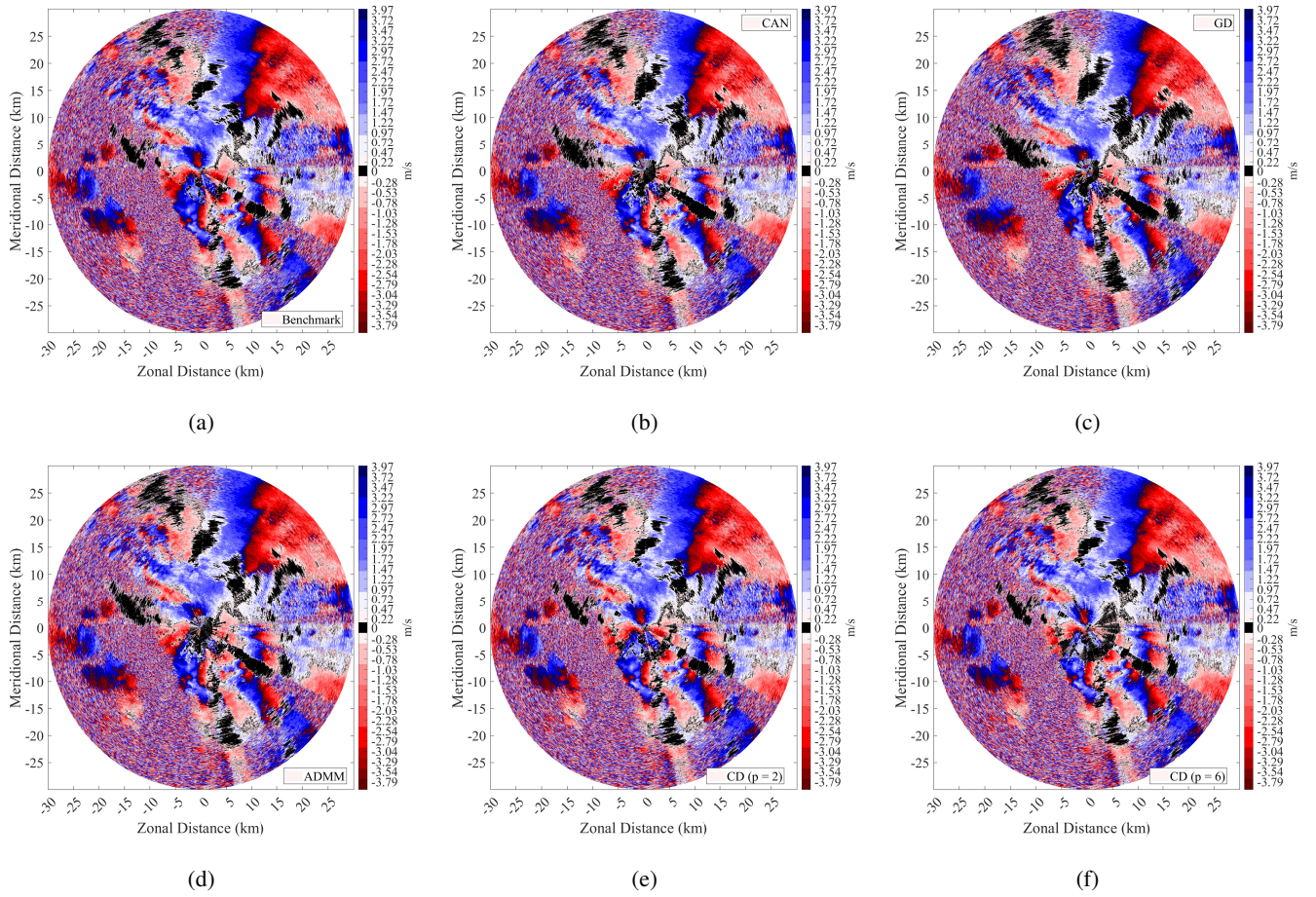
Figure 5: Assessing the radial velocity; (a) Benchmark, (b) CAN, (c) Gradient Descent, (d) ADMM, (e) CD ($p = 2$), and (f) CD ($p = 6$).

minimizing the peak sidelobe level," *Digital Signal Processing*, vol. 116, p. 103142, 2021.

[35] Y. Bu, X. Yu, J. Yang, T. Fan, and G. Cui, "A new approach for design of constant modulus discrete phase radar waveform with low WISL," *Signal Processing*, vol. 187, p. 108145, 2021.

[36] E. Raei, M. Alaee-Kerahroodi, P. Babu, and M. Bhavani Shankar, "Generalized waveform design for sidelobe reduction in MIMO radar systems," *Signal Processing*, vol. 206, p. 108914, 2023.

[37] J. M. Kurdzo, B. L. Cheong, R. D. Palmer, G. Zhang, and J. B. Meier, "A pulse compression waveform for improved-sensitivity weather radar observations," *Journal of Atmospheric and Oceanic Technology*, vol. 31, no. 12, pp. 2713 – 2731, 2014. [Online]. Available: https://journals.ametsoc.org/view/journals/atot/31/12/jtech-d-13-00021_1.xml

[38] C. Pang, P. Hoogeboom, F. Le Chevalier, H. W. J. Russchenberg, J. Dong, T. Wang, and X. Wang, "A pulse compression waveform for weather radars with solid-state transmitters," *IEEE Geoscience and Remote Sensing Letters*, vol. 12, no. 10, pp. 2026–2030, 2015.

[39] L. Rui, H. Jianxin, S. Zhao, F. Xingang, T. Shunxian, and L. Xuehua, "Performance analyses of xy-a solid-state weather radar," in *2017 IEEE International Geoscience and Remote Sensing Symposium (IGARSS)*, 2017, pp. 5994–5997.

[40] F. Argenti and L. Facheris, "Radar pulse compression methods based on nonlinear and quadratic optimization," *IEEE Transactions on Geo-science and Remote Sensing*, vol. 59, no. 5, pp. 3904–3916, 2021.

[41] Q. Xie, H. Zeng, Z. Mo, and W. Li, "A two-step optimization framework for low sidelobe nlfm waveform using fourier series," *IEEE Geoscience and Remote Sensing Letters*, vol. 19, pp. 1–5, 2022.

[42] F. Wang, J. Yin, C. Pang, Y. Li, and X. Wang, "A unified framework of doppler resilient sequences design for simultaneous polarimetric radars," *IEEE Transactions on Geoscience and Remote Sensing*, vol. 60, pp. 1–15, 2022.

[43] F. Wang, S. Feng, J. Yin, C. Pang, Y. Li, and X. Wang, "Unimodular sequence and receiving filter design for local ambiguity function shaping," *IEEE Transactions on Geoscience and Remote Sensing*, vol. 60, pp. 1–12, 2022.

[44] M. Alaee, A. Aubry, A. De Maio, M. M. Naghsh, and M. Modarres-Hashemi, "Design of binary sequences with low PSL/ISL," in *2017 25th European Signal Processing Conference (EUSIPCO)*, 2017, pp. 2211–2215.

[45] M. Alaee-Kerahroodi, M. Modarres-Hashemi, M. M. Naghsh, B. Shankar, and B. Ottersten, "Binary sequences set with small ISL for MIMO radar systems," in *2018 26th European Signal Processing Conference (EUSIPCO)*, 2018, pp. 2395–2399.

[46] P. Stoica, H. He, and J. Li, "Optimization of the receive filter and transmit sequence for active sensing," *IEEE Transactions on Signal Processing*, vol. 60, no. 4, pp. 1730–1740, 2012.
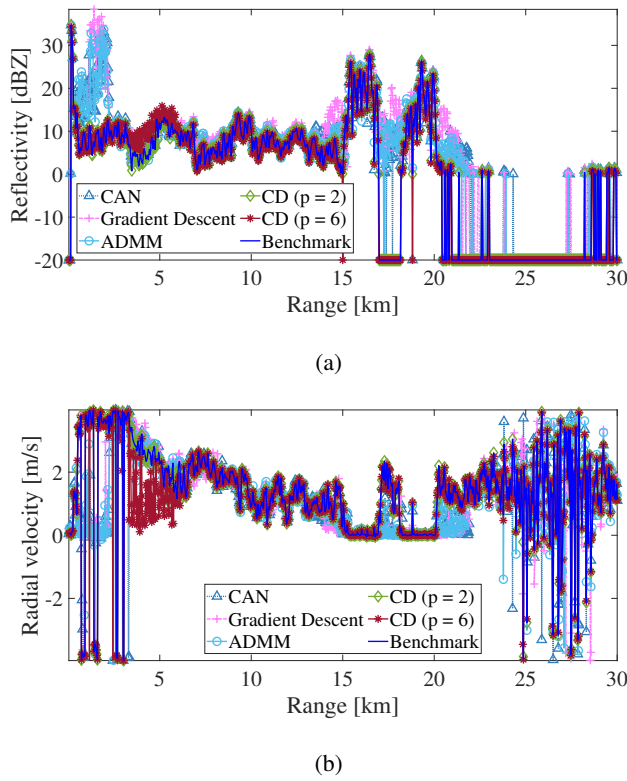
(a)



(b)

Figure 6: Reflectivity level estimation by performing pulse compression on real data at angle cut 7.0807 degree, based on ADMM, CD ($p = 2$), CD ($p = 6$), CAN, and Gradient Descent waveforms. (a) Reflectivity levels. (b) Radial velocity. The figure shows only CD ($p = 2$) due to very low correlation sidelobes is able to closely match the benchmark.

*Signal Processing*, vol. 57, no. 4, pp. 1415–1425, 2009.

[54] J. M. Baden, "Efficient optimization of the merit factor of long binary sequences," *IEEE Transactions on Information Theory*, vol. 57, no. 12, pp. 8084–8094, Dec 2011.

[55] M. Soltanalian and P. Stoica, "Designing unimodular codes via quadratic optimization," *IEEE Transactions on Signal Processing*, vol. 62, no. 5, pp. 1221–1234, March 2014.

[56] J. Song, P. Babu, and D. P. Palomar, "Optimization methods for designing sequences with low autocorrelation sidelobes," *IEEE Transactions on Signal Processing*, vol. 63, no. 15, pp. 3998–4009, Aug 2015.

[57] J. Song, P. Babu, and D. P. Palomar, "Sequence design to minimize the weighted integrated and peak sidelobe levels," *IEEE Transactions on Signal Processing*, vol. 64, no. 8, pp. 2051–2064, 2016.

[58] S. P. Sankuru, R. Jyothi, P. Babu, and M. Alaee-Kerahroodi, "Designing sequence set with minimal peak side-lobe level for applications in high resolution radar imaging," *IEEE Open Journal of Signal Processing*, vol. 2, pp. 17–32, 2021.

[59] E. Raei, M. Alaee-Kerahroodi, and M. B. Shankar, "Spatial- and range-islr trade-off in MIMO radar via waveform correlation optimization," *IEEE Transactions on Signal Processing*, vol. 69, pp. 3283–3298, 2021.

[60] S. P. Sankuru, P. Babu, and M. Alaee-Kerahroodi, "Unipol: Unimodular sequence design via a separable iterative quartic polynomial optimization for active sensing systems," *Signal Processing*, vol. 190, p. 108348, 2022.

[61] C.-Y. Chen and P. P. Vaidyanathan, "MIMO radar waveform optimization with prior information of the extended target and clutter," *IEEE Transactions on Signal Processing*, vol. 57, no. 9, pp. 3533–3544, 2009.

[62] J. Liu, H. Li, and B. Himed, "Joint optimization of transmit and receive beamforming in active arrays," *IEEE Signal Processing Letters*, vol. 21, no. 1, pp. 39–42, 2014.

[63] P. Setlur and M. Rangaswamy, "Waveform design for radar STAP in signal dependent interference," *IEEE Transactions on Signal Processing*, vol. 64, no. 1, pp. 19–34, 2016.

[64] B. Tang and J. Tang, "Joint design of transmit waveforms and receive filters for MIMO radar space-time adaptive processing," *IEEE Transactions on Signal Processing*, vol. 64, no. 18, pp. 4707–4722, 2016.

[65] X. Cheng, A. Aubry, D. Ciuonzo, A. De Maio, and X. Wang, "Robust waveform and filter bank design of polarimetric radar," *IEEE Transactions on Aerospace and Electronic Systems*, vol. 53, no. 1, pp. 370–384, 2017.

[66] Z. Cheng, Z. He, B. Liao, and M. Fang, "MIMO radar waveform design with PAPR and similarity constraints," *IEEE Transactions on Signal Processing*, vol. 66, no. 4, pp. 968–981, 2018.

[67] L. Wu, P. Babu, and D. P. Palomar, "Transmit waveform/receive filter design for MIMO radar with multiple waveform constraints," *IEEE Transactions on Signal Processing*, vol. 66, no. 6, pp. 1526–1540, 2018.

[68] J. Qian, M. Lops, L. Zheng, X. Wang, and Z. He, "Joint system design for coexistence of MIMO radar and MIMO communication," *IEEE Transactions on Signal Processing*, vol. 66, no. 13, pp. 3504–3519, 2018.

[69] S. M. O'Rourke, P. Setlur, M. Rangaswamy, and A. L. Swindlehurst, "Quadratic semidefinite programming for waveform-constrained joint filter-signal design in STAP," *IEEE Transactions on Signal Processing*, vol. 68, pp. 1744–1759, 2020.

[70] K. Zhou, D. Li, Y. Su, and T. Liu, "Joint design of transmit waveform and mismatch filter in the presence of interrupted sampling repeater jamming," *IEEE Signal Processing Letters*, vol. 27, pp. 1610–1614, 2020.

[71] Y. Sun, H. Fan, J. Wang, L. Ren, E. Mao, and T. Long, "Optimization of diverse PCFM waveforms and joint mismatched filters," *IEEE Transactions on Aerospace and Electronic Systems*, vol. 57, no. 3, pp. 1840–1854, 2021.

[72] C. G. Tsinos, A. Arora, S. Chatzinotas, and B. Ottersten, "Joint transmit waveform and receive filter design for dual-function radar-
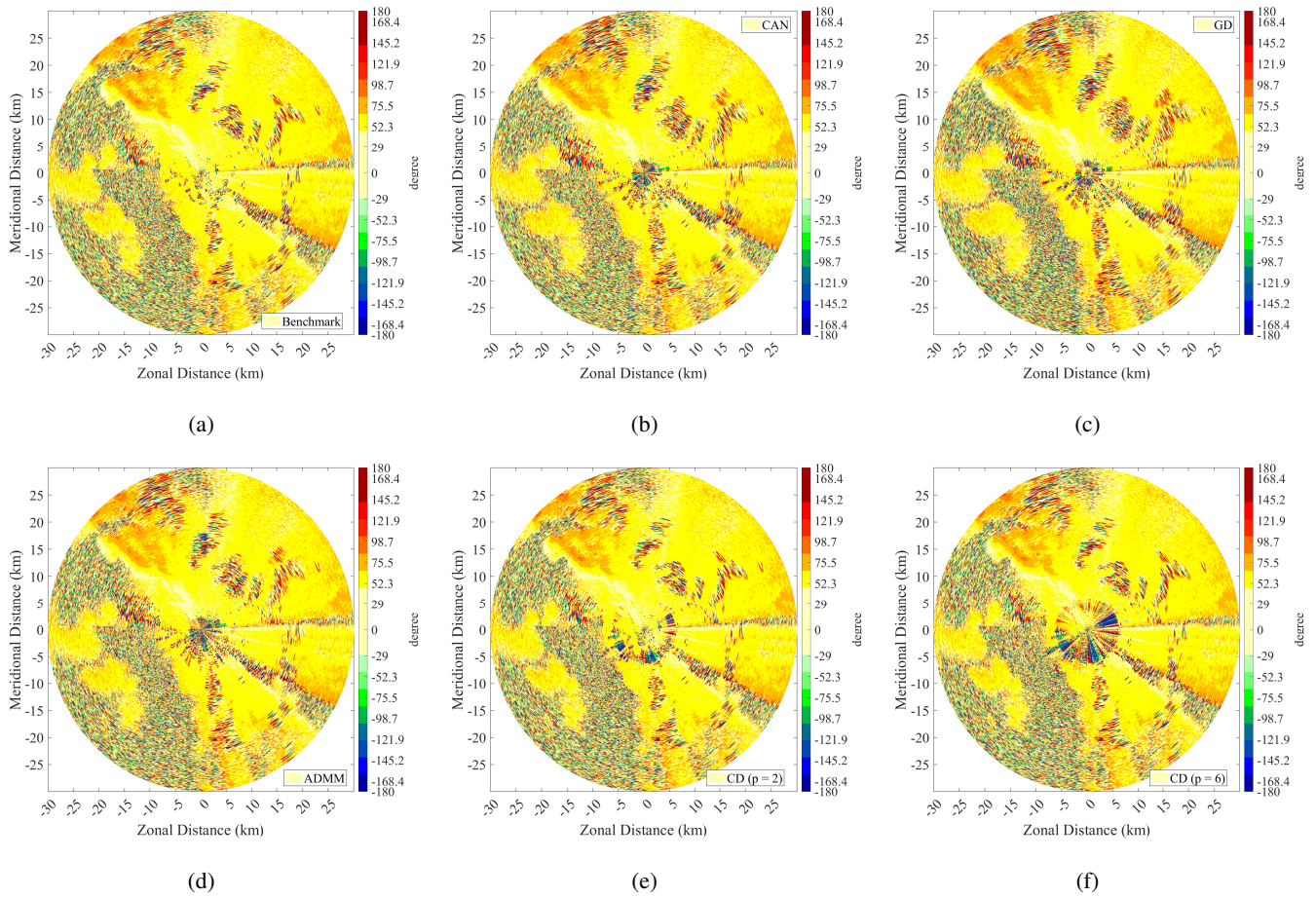
[47] E. Raei, M. Alaee-Kerahroodi, and M. R. Bhavani Shankar, "ADMM based transmit waveform and receive filter design in cognitive radar systems," in *2020 IEEE Radar Conference (RadarConf20)*, 2020, pp. 1–6.

[48] C. D. Curtis and S. M. Torres, "Real-time measurement of the range correlation for range oversampling processing," *Journal of Atmospheric and Oceanic Technology*, vol. 30, no. 12, pp. 2885 – 2895, 2013. [Online]. Available: https://journals.ametsoc.org/view/journals/atot/30/12/jtech-d-13-00090_1.xml

[49] S. M. Torres, C. D. Curtis, and D. Schvartzman, "Requirement-driven design of pulse compression waveforms for weather radars," *Journal of Atmospheric and Oceanic Technology*, vol. 34, no. 6, pp. 1351 – 1369, 2017. [Online]. Available: https://journals.ametsoc.org/view/journals/atot/34/6/jtech-d-16-0231.1.xml

[50] P. Stoica, J. Li, and M. Xue, "On binary probing signals and instrumental variables receivers for radar," *IEEE Transactions on Information Theory*, vol. 54, no. 8, pp. 3820–3825, 2008.

[51] ——, "Transmit codes and receive filters for radar," *IEEE Signal Processing Magazine*, vol. 25, no. 6, pp. 94–109, 2008.

[52] S. J. Frasier, F. Argenti, and L. Facheris, "Predistortion for very low pulse-compression sidelobes in solid-state meteorological radar," *IEEE Geoscience and Remote Sensing Letters*, vol. 20, pp. 1–5, 2023.

[53] P. Stoica, H. He, and J. Li, "New algorithms for designing unimodular sequences with good correlation properties," *IEEE Transactions on*

Figure 7: Differential phase; (a) Benchmark, (b) CAN, (c) Gradient Descent, (d) ADMM, (e) CD ($p = 2$), and (f) CD ($p = 6$).

communication systems," *IEEE Journal of Selected Topics in Signal Processing*, pp. 1–1, 2021.

[73] M. S. Greco, F. Gini, P. Stinco, and K. Bell, "Cognitive radars: On the road to reality: Progress thus far and possibilities for the future," *IEEE Signal Processing Magazine*, vol. 35, no. 4, pp. 112–125, 2018.

[74] A. D. Byrd, I. R. Ivić, R. D. Palmer, B. M. Isom, B. L. Cheong, A. D. Schenkman, and M. Xue, "A weather radar simulator for the evaluation of polarimetric phased array performance," *IEEE Transactions on Geoscience and Remote Sensing*, vol. 54, no. 7, pp. 4178–4189, 2016.

[75] M. E. Levanon Nadav, *Radar Signals*. John Wiley & Sons, Inc., Publication, 2004.

[76] ELDES S.r.l. , "X-band dual polarization and doppler - ELDES - radar," Jun 2021. [Online]. Available: https://www.eldesradar.com/wp-content/uploads/2022/08/WR-25XP-Brochure-rev-8.0.pdf

**Mohammad Alaee-Kerahroodi** completed his PhD in telecommunication engineering at the Department of Electrical and Computer Engineering in 2017 from Isfahan University of Technology, Iran. In 2016, he also served as a visiting researcher at the University of Naples "Federico II" in Italy. After obtaining his doctorate, he joined the Interdisciplinary Centre for Security, Reliability, and Trust (SnT) at the University of Luxembourg, Luxembourg, as a research associate. Currently, he holds the position of a research scientist at SnT, where he leads the prototyping and laboratory activities for the SPARC (Signal Processing Applications in Radar and Communications) research group. His research focuses on radar waveform design and array signal processing, with a particular interest in developing innovative solutions for 4D-imaging millimeter wave MIMO radar sensors. Dr. Alaee brings a wealth of practical experience to his research, having spent over 12 years extensively engaged with various radar systems. His expertise spans multiple radar related domains, including automotive radar, ground surveillance radar, air surveillance radar, weather monitoring radar, passive sensing radar, and marine radar applications.
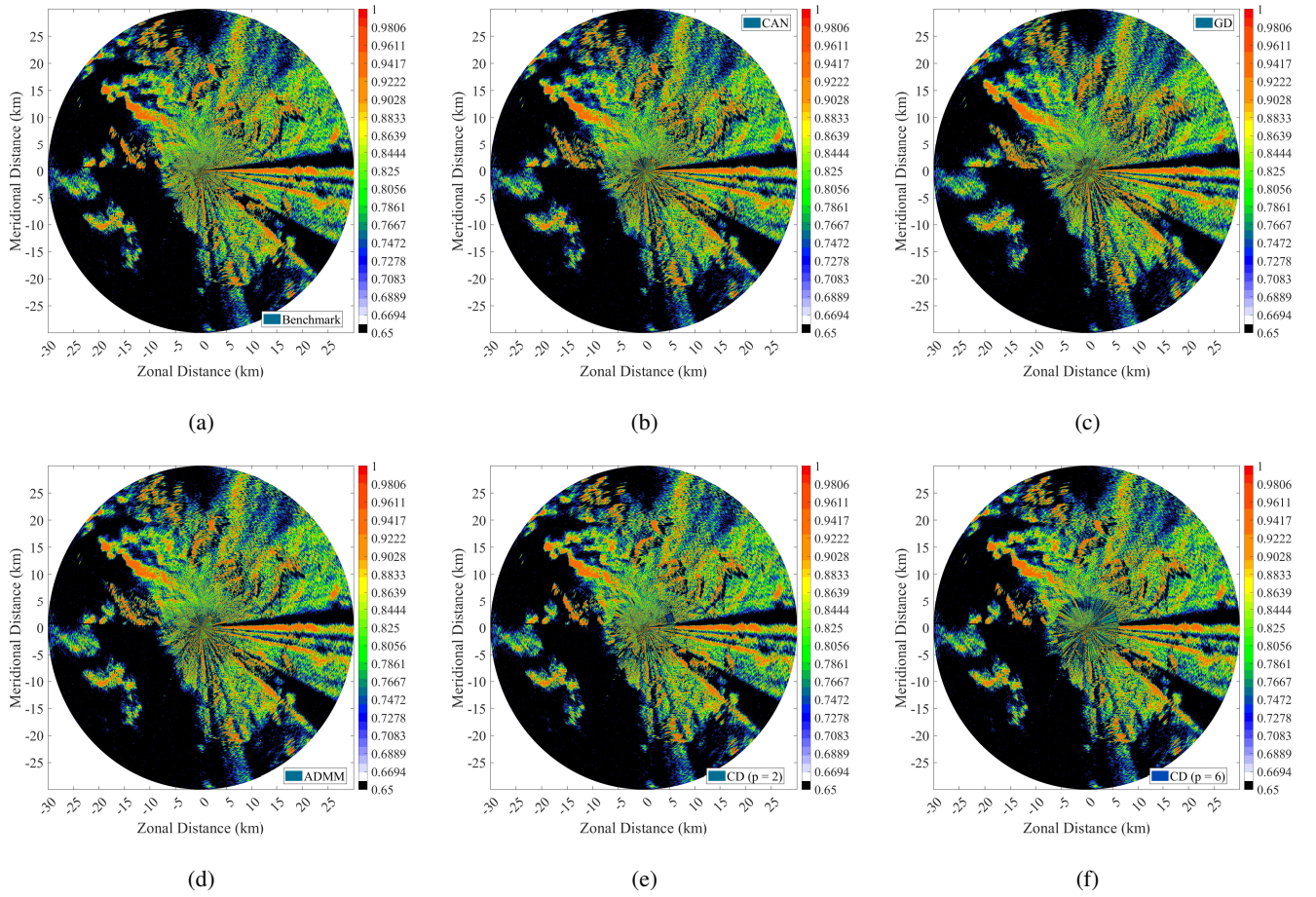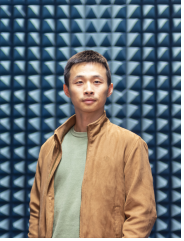
Figure 8: Correlation coefficient; (a) Benchmark, (b) CAN, (c) Gradient Descent, (d) ADMM, (e) CD ($p = 2$), and (f) CD ($p = 6$).

**Linlong Wu** received the B.E. degree in electronic information from Xi'an Jiaotong University (XJTU), Xi'an, China, in 2014, and the Ph.D. degree in electronic and computer engineering from Hong Kong University of Science and Technology (HKUST), Hong Kong, in 2018. He was with the wireless network group of Alibaba Cloud from November 2018 to October 2020 as a Research Engineer working on designing and building commercial RFID based localization systems. Since November, 2020, he has been with the Interdisciplinary Centre for Security, Reliability and Trust (SnT), University of Luxembourg and is currently a Research Associate in the Signal Processing Applications in Radar and Communications (SPARC) group. His research interests are signal processing, optimization and machine learning with applications in waveform design, integrated sensing and communication and IoT networks.

**Ehsan Raei** received his M.Sc. degree in Telecommunications Engineering from Isfahan University of Technology (IUT), Iran, in 2014. He joined Signal Processing Applications in Radar and Communications (SPARC) group, Interdisciplinary Centre for Security, Reliability, and Trust (SnT), University of Luxembourg as a Ph.D. candidate in 2018. He received his Ph.D. in June 2022. After defending his doctorate, he continued collaboration with the SPARC group of SnT as a research associate from June 2022 to January 2023. He joined Amphinicy Technologies company as a Senior Digital Signal Processing (DSP) Architect in January 2023, and currently, he is working on implementing DSP blocks for Satellite Communication (SATCOM) applications. His research interests include radar waveform design, MIMO radars, radar array processing, automotive radars, imaging radar, optimization, detection, estimation, signal processing, SATCOM, and Software Defined Radio (SDR).

**M. R. Bhavani Shankar** received Masters and Ph. D in Electrical Communication Engineering from Indian Institute of Science, Bangalore in 2000 and 2007 respectively. He was a Post Doc at the ACCESS Linnaeus Centre, Signal Processing Lab, Royal Institute of Technology (KTH), Sweden from 2007 to September 2009. He joined SnT in October 2009 as a Research Associate and is currently a Senior Research Scientist/ Assistant Professor at SnT leading the SPARC (Signal Processing Applications in Radar and Communications). He was with Beceem Communications, Bangalore from 2006 to 2007 as a Staff Design Engineer working on Physical Layer algorithms for WiMAX compliant chipsets. He was a visiting student at the Communication Theory Group, ETH Zurich, headed by Prof. Helmut Bölcskei during 2004. Prior to joining Ph. D, he worked on Audio Coding algorithms in Sasken Communications, Bangalore as a Design Engineer from 2000 to 2001. His research interests include Design and Optimization of MIMO Communication Systems, Automotive Radar and Array Processing, polynomial signal processing, Satellite communication systems, Resource Allocation and Fast Algorithms for Structured Matrices.

He is currently the Chair of the IEEE Benelux joint chapter on communications and vehicular technology, member of the Sensor Array Mulichannel (SAM) Technical Committee of Signal Processing Society, serves as handling editor for Elsevier Signal Processing and member of the EURASIP Technical Area Committee on Theoretical and Methodological Trends in Signal Processing. He was a co-recipient of the 2014 Distinguished Contributions to Satellite Communications Award, from the Satellite and Space Communications Technical Committee of the IEEE Communications Society.